Porous and rough micro/nano structures for enhancing the performance of phase change cooling systems

by

Soroush Niazi

Submitted to the Graduate School of Natural Science and Engineering
In partial fulfillment of the requirement for the degree of
Master of Science

Sabanci University
July 2021

Porous and rough micro/nano structures for enhancing the performance of phase change cooling systems

APPROVED BY:

DATE OF APPROVAL: 14/07/2021

ABSTRACT

Porous and rough micro/nano structures for enhancing the performance of phase change cooling systems

SOROUSH NIAZI

Mechatronics Engineering, M.Sc. Thesis, July 2021

Thesis Advisors: Prof. Ali Koşar & Dr. Abdolali Khalili Sadaghiani

Keywords: Bio-coating, Heat transfer enhancement, Environmentally friendly coatings, Electronics cooling, Air conditioning system

Due to growing cooling demands as well as emerging global warming and climate change issues, cooling systems should be more efficiently utilized. Boiling is an effective heat transfer mechanism, which has a critical role in many cooling systems. Surface modification is considered as the major approach for boiling heat transfer enhancement. In this thesis, we developed a microbial bio-coating surface modification technique for phase change cooling applications. Thermoacidophilic Sulfolobus solfataricus coating was implemented using a facile dip coating method on different metallic and non-metallic surfaces. Controlled by drying conditions, the coating exhibited rough and porous morphologies. When tested in a boiling heat transfer setup, bio-coated surfaces offered enhancements up to 76.3% in Critical Heat Flux (CHF). Next, a miniature evaporator was coated and tested for real-world air-conditioning applications, and coefficient of performance (COP) enhancements up to 11% clearly revealed the potential of bio-coated surfaces for energy saving purpose and reduction in greenhouse gasses. Furthermore, coated evaporators reduced the exergy destruction rate up to 8%. This thesis not only offers a new type of coating morphology, but the applicability of the proposed bio-coating is also proven in a miniature air conditioning system.

ÖZET

Faz değişimli soğutma sistemlerinin performansını artırmak için gözenekli ve pürüzlü mikro/nano yapılar

SOROUSH NIAZI

Mekatronik Mühendisliği YÜKSEK LİSANS TEZİ, Temmuz 2021

Tez Danışmanı: Prof. Dr. Ali Koşar & Dr. Abdolali Khalili Sadaghiani

Anahtar Kelimeler: Biyo-kaplama, Isı transferini güçlendirme, Çevre dostu kaplamalar, Elektronik soğutma, Klima sistemi

Artan soğutma talepleri ve ortaya çıkan küresel ısınma ve iklim değişikliği sorunları nedeniyle, soğutma sistemleri daha verimli kullanılmalıdır. Kaynama, birçok soğutma sisteminde kritik bir role sahip olan etkili bir ısı transfer mekanizmasıdır. Yüzey modifikasyonu, kaynama ısı transferinin artırılması için ana yaklaşım olarak kabul edilir. Bu tezde, faz değişimli soğutma uygulamaları için bir mikrobiyal biyo-kaplama yüzey modifikasyon tekniği geliştirilmiştir. Termoasidofilik Sulfolobus Solfataricus kaplama, farklı metalik ve metalik olmayan yüzeylerde kolay daldırma kaplama yöntemi kullanılarak uygulanmıştır. Kuruma koşullarını geciktiren kaplamalar, pürüzlü ve gözenekli morfolojiler sergilemiştir. Kaynama ısı transferi düzeneğinde test edildiğinde, biyo-kaplanmış yüzeyler Kritik Isı Akışında (CHF) %76.3'e varan iyileştirmeler sunmuştur. Daha sonra, minyatür bir evaporatör kaplanmış ve gerçek iklimlendirme uygulamaları için test edilmiştir. %11'e varan performans katsayısı (COP) geliştirmeleri elde edilmiş, enerji tasarrufu amaçları ve sera gazlarında azalma için biyo-kaplamalı yüzeylerin potansiyeli açıkça ortaya konulmuştur. Ayrıca, kaplamalı evaporatörler ekserji yıkım oranını %8'e kadar azaltmıştır. Bu tez, yalnızca yeni bir kaplama morfolojisi türü önermekle kalmamakta, aynı zamanda önerilen biyo-kaplamanın uygulanabilirliği minyatür bir iklimlendirme sisteminde de kanıtlanmaktadır.

ACKNOWLEDGEMENTS

First of all, I am deeply thankful to my supervisors, Prof. Dr. Ali Koşar and Dr. Abdolali Khalili Sadaghiani, for offering their unlimited supports, guidance, and sharing their valuable experiences and knowledge during my Master's studies.

I would like to thank my honorable jury members: Dr. Özlem Kutlu form SUNUM, and Dr. Yegân Erdem from Bilkent University for their input and valuable comments.

I would like to thank Sabanci University, SUNUM, and TUBITAK. The performed research was supported by the Turkish Scientific and Technological Council (TUBITAK) 2247B support (Grant number: 119C026).

Finally, I would like to thank my beloved family for their unconditional love, support and dedications through this progress. A special thanks goes to all my dear friends especially Moein Talebian Gevari, Taher Abbasiasl, and Milad Shojaeian, who were always there for me in case of any difficulties.

This thesis is dedicated to my beloved family

TABLE OF CONTENTS

LIST OF FIGURES

LIST OF TABLES

NOMENCLATURE

Subscripts and abbreviations:

AC	Air conditioning system
AFM	Atomic Force Microscopy
BHT	Boiling heat transfer
COP	Coefficient of performance
CHF	Critical heat flux
cond	Condenser
dest	Destruction
ev	Evaporator
EPS	Extracellular polymeric substance
HTC	Heat transfer coefficient
in	Inlet
ID	Inner diameter
ONB	Onset nucleate boiling
OD_{600}	Optical density at wavelength of 600 nm
OD	Outer diameter
out	Outlet
PBS	Phosphate-buffered saline
PPI	Pore number per inch
pre	Preheater
SEM	Scanning electron microscopy
WCA	Water contact angle method

Symbols:

A	Heated area [m^2]
C_p	Heat Capacity [J/K]
h	Heat transfer coefficient [W/cm^{2}K]
h	Enthalpy [kJ/kg]
I	Current [A]
K	Thermal conductivity [W/mK]
P	Pressure [kPa]
R	Thermal resistance [m^{2}K/W]
S	Entropy [kJ/kgK]
T	Temperature [K]
T_0	Ambient temperature [K]
T_s	Surface temperature [K]
T_{sat}	Saturation temperature [K]
V	Voltage [V]
x	Vapor quality
ΔT	Wall superheat [K]
W	Consumed work by the system [W]
Q_c	Heat by the heat source [W]
q''	Net heat flux [W/cm^2]
$\dot{m}$	Mass flow rate [kg/s]
$\dot{E}$	Exergy [W]

1 CHAPTER ONE: INTRODUCTION

1.1 Global Cooling demands

Global warming, as a direct consequence of the increase in greenhouse gas emission, has remained the main worldwide concern during the last decades. Heat loss is the predominant form of the energy lost in energy systems/processes. One of the major sources of energy losses is linked with the constant utilization of air conditioning, refrigeration, and heat pipe systems. According to the International Energy Agency (IEA), the cooling demands in the air conditioning market are predicted to be tripled by 2050 [1]. It is reported that the average efficiency of the air conditioning systems is about 50%. It means that half of the energy is wasted during the energy transformation process. Thus, many attempts have been made to enhance the energy efficiency of these systems.

1.2 Boiling heat transfer as an effective solution

Due to its ability to remove large quantities of heat, boiling phenomenon is used as a cooling method in air conditioning and refrigeration systems [2],[3]. Despite its superiorities compared to the conventional methods, boiling has a limit called critical heat flux (CHF), where the vapor columns create a vapor blanket film on the surface, which drastically decreases the heat transfer rate from the surface. Figure 1.1 shows the typical boiling regimes. First, natural convection corresponding to single phase flow happens. The boiling process starts with the inception of bubbles from the nucleation sites on the heated surface (cavities and surface impurities). Here, the required temperature for the onset of nucleate boiling (ONB) depends on the surface morphology. As the surface temperature increases, nucleate boiling regime, a region characterized by more activated nucleation sites and discrete departed bubbles, starts. A further surface temperature increase results in more generated bubbles leaving the surface in the forms of vapor columns and larger bubbles. The end of the nucleate boiling region is described by excessive generated vapor columns and blankets, which block the coolant path to the surface, thereby leading to boiling crisis or critical heat flux (CHF). As indicated in Figure 1.1, boiling heat transfer enhancement can be achieved by i) reducing ONB temperature, ii) improving heat transfer coefficient (HTC), and iii) increasing CHF [4]. Changing the working fluid and using Nanofluids in thermal systems [5] is one of the widely used techniques in the literature, but it has some issues such as sedimentation [6]. Thus, surface modification is one of the best approach with minimum drawbacks for enhancing the boiling heat transfer.

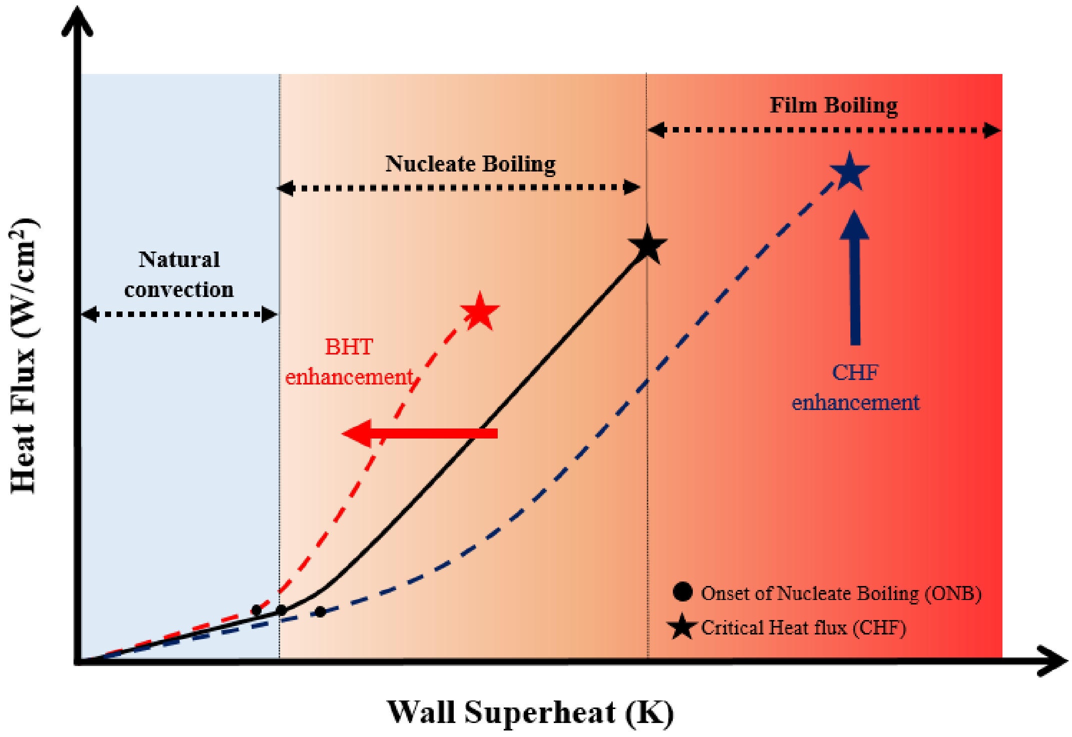

Figure 1.1. Boiling regimes, boiling heat transfer (BHT) and critical heat flux (CHF) enhancements in an ideal boiling curve.

1.3 Surface modification techniques

Many surface modification techniques [7][8] have been proposed and investigated to achieve these goals. These techniques include implementation of nanowire arrays [9][10][11], nanorods [12], graphene coating [13], polymeric coating [14][15][16], virus coating [17], biphilic surfaces [18], porous surfaces [19][20], laser-engineered surfaces [21], and plasma spray coating [22]. Based on the application and the range of the applied heat fluxes, these three aspects should be considered in the design of thermal-fluids systems to maximize the heat removal from the surface in nucleate boiling and film boiling regimes.

1.3.1 Literature review on rough enhanced surfaces

As an example for surface modification, Ma et al. [23] investigated surface area enhancement in flow boiling via micro-pin-fins. The surface revealed the effect of fin height, fluid velocity and liquid sub-cooling on heat transfer. Sadaghiani et al. [24] explored the effect of copper based micro- and nano-structured surfaces on flow boiling. Alam et al. [25] studied the effect of surface roughness on flow boiling. These studies showed that the roughness elements about the size of 1 and 1.6 μm considerably affected the nucleation site density and boiling inception. Roughness elements can majorly be introduced via mechanical modification such as sanding, etching, and deposition [8]. In the study conducted by Jung et al. [26], the effects of treated surfaces by anodization in two acids as the electrolyte (deposition) and with submicron-roughness on subcooled flow boiling of FC-72 were investigated at ambient pressure. Their observations marked an increase in HTC and CHF. Sisman et al. [27] applied roughness with the size of 1 to 4μm on aluminum sheets with the mechanical sanding technique and reported that smaller roughness could create more active nucleation sites at the same heat fluxes.

1.3.2 Literature review on porous enhanced surfaces

In addition to roughness, tuning the porosity is one of the widely used modification techniques in boiling heat transfer. Porous foams generate a high surface area-to-volume ratio. Rainey et al. [28] investigated the effect of micro-porosity using the ABM coating method (Aluminum particles, Devcon Brushable Ceramic epoxy, and Methyl-Ethyl-Keytone) on subcooled flow boiling of FC-72. Compared to non-coated surfaces, boiling inception took place at lower wall superheats and consequently increased heat transfer coefficients. However, the development of microporous coating using Al_2O_3 particles with size of less than 10μm resulted in 25% CHF enhancement [29]. Further investigation on R-134a flow boiling in tubes with a metallic porous surface exhibited increased heat transfer coefficient (up to 200%), as the cell size of the metal foam was changed from 20 PPI (pore number per inch) to 40 PPI [30]. In the study conducted by Pranoto and Leong [31], high thermal conductivity graphite foams with average pore diameter of 350 and 650 μm were used in flow boiling experiments. As a result, more nucleation sites on the porous surface could be observed, which raised the heat transfer coefficient by 2.5 times.

1.4 Research objectives

As can be seen from the abovementioned studies, the available enhancement methods require expensive infrastructure, have a complex process flow for their fabrication/preparation, and most importantly, cause environmental issues due to released hazardous materials as by-products. On the other hand, according to the latest market report published by fortune business insights, the global paints and coatings market size in 2019 was 154.6 billion USD and is expected to reach an estimated value of 249.7 billion USD in 2027 [32]. This huge budget is mostly based on the demand for new generation coatings and should be wisely managed in order to meet global energy needs.

While the industry is seeking for the energy-efficient components, energy systems are failing to track the progress in clean energy. To fill this gap, this thesis introduces a bio-coating to modify the surface of heat exchangers by providing organic porous and roughened surfaces. The purpose of this study is to generate a paradigm shift in a broader context, by avoiding fossil-based coatings. In this thesis, this next generation bio-coating is implemented to an actual thermal-fluids system. The proposed coating is highly durable, environmentally friendly, and cheap and has a practical coating method for the implementation to thermal-fluids systems [33]. This study not only offers new types of coating morphologies, but also the applicability of the proposed bio-coating is proven with its implementation to a miniature air conditioning system.

2 CHAPTER TWO: EXPERIMENTAL SETUPS AND PROCEDURE

2.1 Pool boiling

Pool boiling is one of the fundamental studies that allows researchers to observe the performance fn any surface structures in terms of hear transfer, bubble formation, bubble coalescence and bubble ascent. In pool boiling tests, the focus is on the bubbles dynamic through the surface without any external force. Although in pool boiling the fluid is stationary,upon boiling and bubbles departure, mixing occurs as a result of bubbles motion. In pool boiling experiments, three regions of boiling are observed: Natural convection (in single phase heat transfer), nucleate boiling and film boiling (Figure 1.1).

2.1.1 Experimental setup

The schematic of the pool boiling setup is shown in Figure 2.1. Four cartridge heaters are installed at the bottom of the test section for providing the desired heat for increasing the surface temperature. One immersion cartridge heater is placed into the pool of water from the top for increasing the temperature of the fluid's bulk up to saturation temperature. The aluminum test section is surrounded by insulation Teflon block to avoid excessive heat loss. Surfaces with the dimension of 15mm×15mm can be placed on top of the aluminum cartridge heater and by five thermocouples beneath the surface; the temperature of the surface can be measured. Glass walls are sandwiched and sealed on top of the Teflon block to prevent any leakage. A reflux condenser is located on top of a hole above the pool, so that the vapors that are generated during the boiling, be condensed and the fluid's volume be constant during the experiments. On top of the condenser, there is a hole to atmosphere in order to keep the tests at the ambient pressure. For attaching the desired surface on top of the aluminum block, thermal paste is used and the thermal resistance of the paste is calculated in the analysis (Section 2.4).

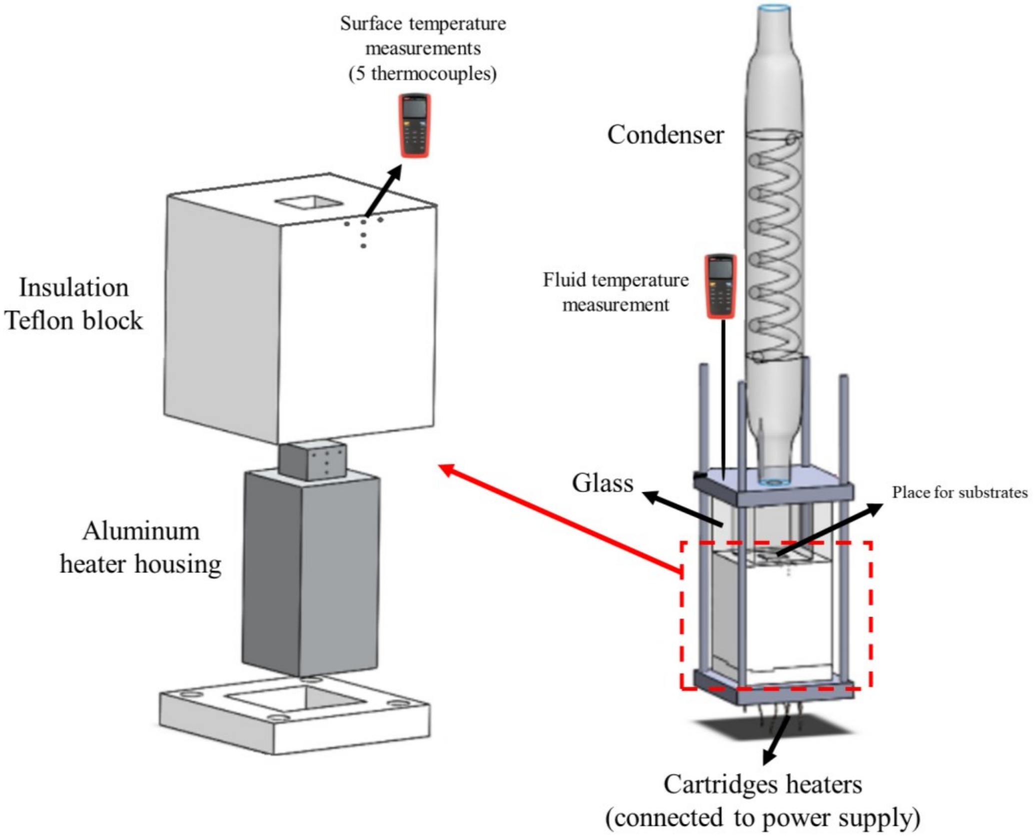

Figure 2.1. Schematic of the pool boiling experimental setup.

2.2 Flow boiling

After obtaining the fundamental results of the engineered surfaces in the pool boiling experiments, they are tested in flow boiling experimental setups since they have superior heat removal ability in flow condition and these tests are required for real-word cooling applications such as electronic cooling. Flow boiling gives us better understating of the actual boiling regimes due to the constant rewetting capability of the working fluid. Although instabilities occur in transition between different flow boiling regimes, it can be concluded that there are mainly four boiling flow patterns namely as bubbly flow, slug flow, annular flow and dryout. [34].

2.2.1 Experimental setup

The schematic and pictures of the flow boiling setup is demonstrated in Figure 2.2. A channel with dimensions of 50×15×0.5 mm^3 and equipped with pressure and temperature sensors was used to perform flow boiling experiments. Two cartridge heaters were used for applying heat from the bottom of the channel. A digital power supply was connected to cartridge heaters, and current and voltage were measured at every heat flux. The test section was made of aluminum. To minimize the heat losses, Teflon was used surrounding the aluminum block. A plexiglass was utilized on top of the channel, which allow the flow visualization from the top. Two holder plates were used on top and bottom of the setup to sandwich the Plexiglass on top of plastic O-rings. A commercial camera, Canon EOS 70D, was used to visualize boiling during heating. Four horizontal holes were formed in the aluminum block under the surface of the minichannel to measure the surface temperatures using T-type thermocouples and UNI-T UT325 Contact thermometers. The bio-coated silicon was located on top of the aluminum block. Deepcool Z3 paste, a superconductive thermal paste, was used for attaching the silicon surface on the aluminum block. A micro gear pump was used to pump the fluid through the system. Deionized water was used as the working fluid. The working fluid was degassed using a vacuum tank to remove dissolved gas from the water by lowering the pressure inside the tank and was then introduced into the preheater section before entering the boiling test section. The preheater was an immersed heat exchanger in 100°C silicon oil whose temperature was controlled with a PID controller.

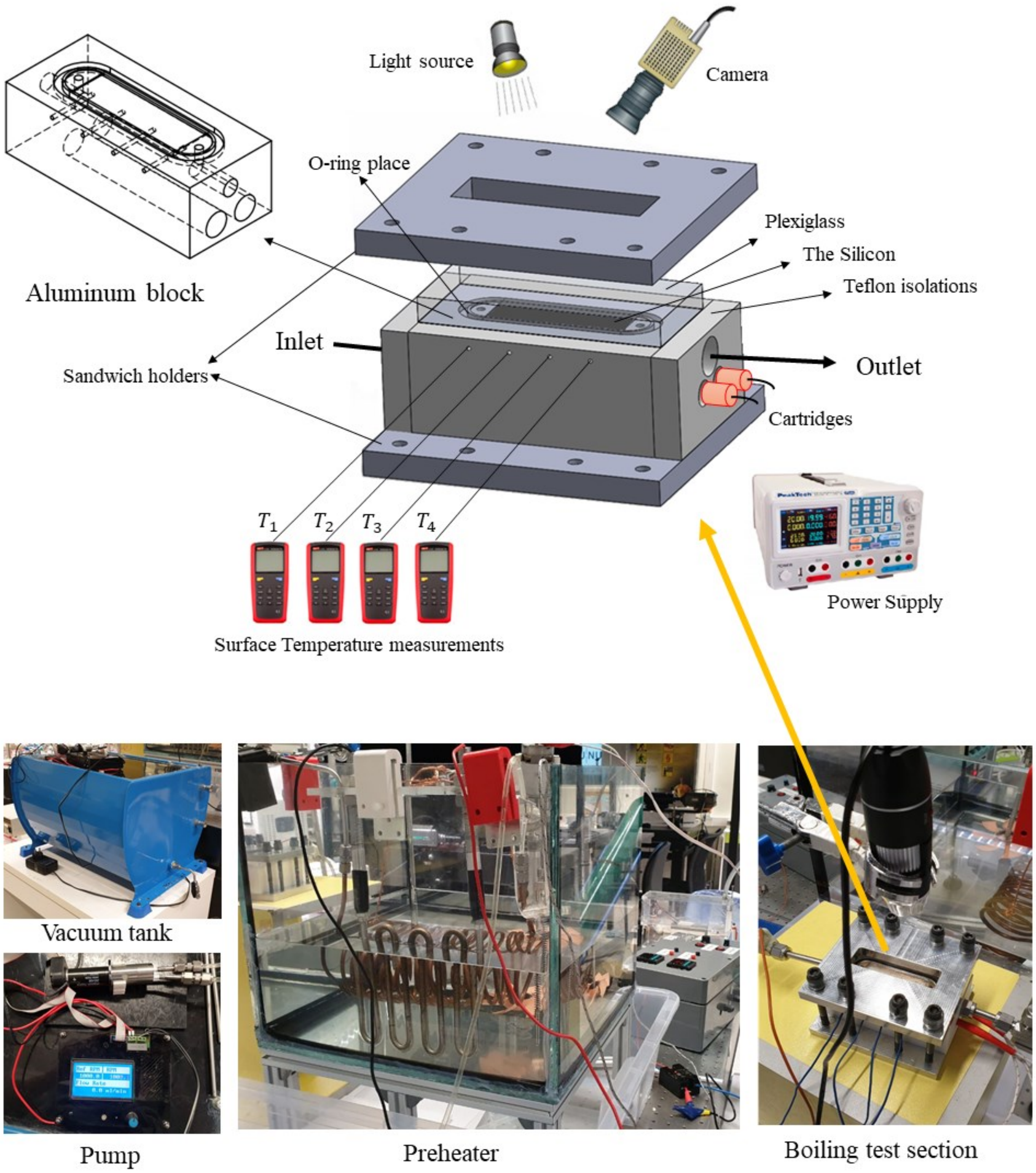

Figure 2.2. Open-loop flow boiling test section.

2.3 Lab-made close-loop air conditioning system

Figure 2.3 depicts the experimental setup of the miniature air conditioning system, which was assembled to measure the cooling performance of the bio-coated aluminum tube. It consists of a condenser, a chiller, a pump, a preheater, a reservoir, valves, and the test section. The temperatures and pressures at different locations were measured using UNI-T UT325 thermometers connected to T-type thermocouples and pressure gauge (Omega). A preheater is placed before the test section to keep the inlet temperature of the coolant at 56°C. Two thermocouples were installed for temperature measurement, one prior to entering the evaporator and the other one at the exit of the evaporator. The test section was a constant temperature chamber, which includes an electrical heater, four thermocouples for air temperature measurements, two thermocouples for coolant temperature measurements, a fan, a spongy pad for heat dissipation and the evaporator. The chamber walls were thermally isolated via 5 mm thick ceramic paper to reduce the thermal losses.

FC-72 was used as the working fluid in this system. The evaporator was made of an aluminum tube with the inner diameter (ID) of 6mm, the outer diameter (OD) of 8mm, and the length of 200 cm. The experiments were performed at four different chamber temperatures. Inside the chamber, an electrical heater fan (2000W) connected to a PID (Proportional Integral Derivative) controller keeps the chamber temperature at a desired constant value. While the electrical heater heats up the chamber, the coolant passing through the evaporator cools down the hot air. A power-meter device was used to obtain the power consumptions. The power consumption of the electrical heater in the chamber was measured for cases of non-coated surface and bio-coated evaporators.

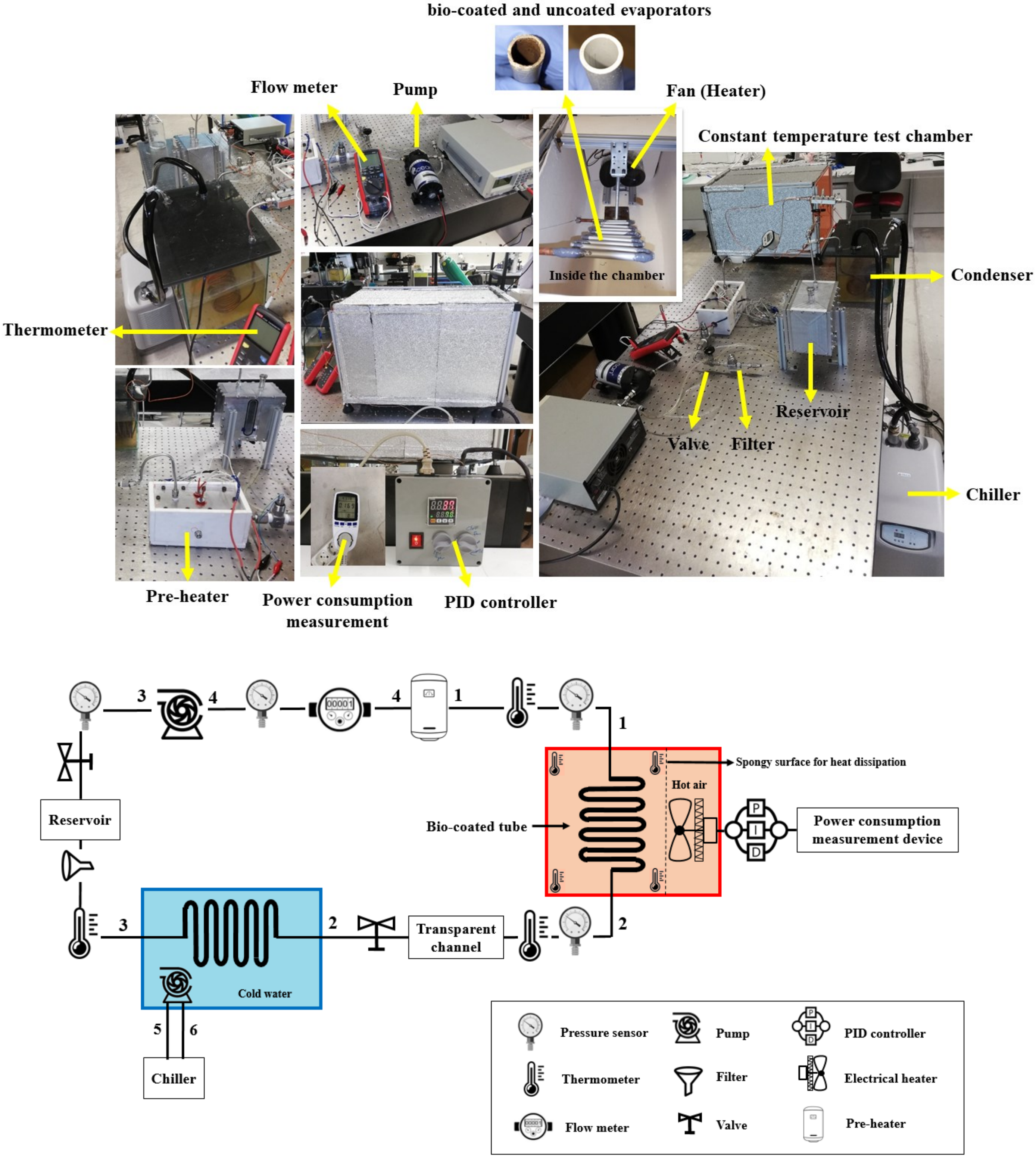

Figure 2.3. Experimental setup of the lab-made miniature air conditioning system and its schematic.

2.4 Analysis method and data reduction

2.4.1 Pool boiling and flow boiling

The porous- and rough-coated surfaces were tested in pool boiling and flow boiling experimental setups to investigate the effect of surface properties on boiling heat transfer and two-phase flow behavior. The experiments on non-coated and bio-coated surfaces in the flow boiling setup were performed under the atmospheric pressure at the mass flux of ~100 kg/m^{2}s (corresponds to typical mass flux of miniature air-conditioning systems [35]). The wall superheats (ΔT_{sat}) – defined as the temperature difference between the surface (T_s) and saturation temperature (T_{sat}) – were obtained for the applied heat inputs. The comparisons of the heat transfer performance between non-coated and coated surfaces are presented in Figure 4.1. It should be noted that each test was repeated for three times to ensure the repeatability of the experiments. The local heat transfer coefficient is calculated as:

$$h = \frac{1}{A}\frac{Q}{\Delta T_{sat}} \tag{2.1}$$

In equation 2.1, Q is the net heat input (W), ΔT_{sat} is the wall superheat (K), and A is the surface area (m^2). Four temperature measurements were used to calculate the average temperature of the surface in the aluminum block (at 4 mm beneath the substrates). The average of the measurements was used as the surface average temperature in flow boiling experimental setup:

$$T_{\,average} = \frac{T_1 + T_2 + T_3 + T_4}{4} \tag{2.2}$$

The net heat flux, heat loss, and surface temperatures are calculated using equations (2.3) to (2.5):

$$q'' = \frac{IV - Q_{Loss}}{A} \tag{2.3}$$

$$Q_{Loss} = IV - \dot{m}c_p\Delta T = \ Heat\ loss\ percentage\ \times\ IV \tag{2.4}$$

$$T_{surface} = T_{average} - q''(\frac{L_{Al}}{K_{AL}} + \frac{L_{Silicon}}{K_{Silicon}} + R_{paste}) \tag{2.5}$$

where I, V, and A are the applied current (A), voltage(V), and the heated area (m^2), respectively. Heat loss is the difference between input power and the amount of heating needed at a specified mass flow rate at a constant ΔT. The percentage of the heat loss in the boiling setup was calculated less than 8%. L_{Al} is the vertical length between surface temperature measurement location and substrate, and $L_{Silicon}$ is thickness of the silicon wafer, which is 500 µm. K is the thermal conductivity, and $R_{paste} = 6 \times 10^{-6}\ \frac{m^2k}{W}$ is the thermal resistance of the thermal paste used to reduce the thermal resistance between two surfaces.

2.4.2 Lab-made air conditioning system

The consumed work by the system is the sum of pumping power, preheater power and the chiller power. The pumping power kept constant at 10.2 W for pumping the fluid at flow rate of 1.66 ml/s and mass flux of 100 kg/m^2s. The preheater connected to a power supply consumed 110W to increase the fluid's temperature from 23°C to 56°C. The condenser connected to a chiller use 220W to reduce the temperature of the heated fluid to 23°C.

Second law analysis was performed on the system components of the Lab-made close loop Air Conditioning system to investigate the effect of bio-coating on exergy destruction rate. The following expression can be written based on the general exergy balance [36]:

$$\dot{E}_{dest} = \dot{E}_{in} - \dot{E}_{out} = \dot{m}(e_{in} - e_{out}) \tag{2.6}$$

where $\dot{E}_{in}$ and $\dot{E}_{out}$ are the total exergy (transferred by heat, work and mass) at the inlet and outlet, respectively, and $\dot{E}_{dest}$ is the rate of exergy destruction. For the ambient temperature of T_0 and assuming that the change in kinetic and potential energies is negligible, the exergy is given as:

$$e = (h - h_0) - T_0(S - S_0) \tag{2.7}$$

The component-wise analysis for the air conditioning system including evaporator, condenser, preheater and pump are as follows:

- Evaporator:

$$\dot{E}_{dest,ev} = \left(\dot{E}_1 - \dot{E}_2\right) + \dot{Q}_c\left(1 - \frac{T_0}{T_L}\right) \tag{2.8}$$

$$= \dot{m}(h_1 - T_0S_1) - \dot{m}(h_2 - T_0S_2) + \dot{Q}_L\left(1 - \frac{T_0}{T_L}\right)$$

- Condenser:

$$\dot{E}_{dest,cond} = \left(\dot{E}_2 - \dot{E}_3\right) + \left(\dot{E}_5 - \dot{E}_6\right) \tag{2.9}$$

$$= \dot{m}(h_2 - T_0S_2) - \dot{m}(h_3 - T_0S_3) + \dot{m}(h_5 - T_0S_5) - \dot{m}(h_6 - T_0S_6)$$

- Pump:

$$\dot{W}_{pump} = \dot{m}(h_3 - h_4) \tag{2.10}$$

$$\dot{E}_{dest,pump} = \left(\dot{E}_3 - \dot{E}_4\right) + \dot{W}_{pump} = \dot{m}(T_0(S_4 - S_3)) \tag{2.11}$$

- Preheater:

$$\dot{E}_{dest,pre} = \left(\dot{E}_1 - \dot{E}_4\right) = \dot{m}(h_1 - T_0S_1) - \dot{m}(h_4 - T_0S_4) \tag{2.12}$$

- Total:

$$\dot{E}_{dest,tot} = \dot{E}_{dest,ev} + \dot{E}_{dest,cond} + \dot{E}_{dest,pump} + \dot{E}_{dest,pre} \tag{2.13}$$

The following assumptions are made in the thermodynamic analysis:

a) The effects of variation in the kinetic and potential energy are assumed to be negligible during the flow of refrigerants throughout the system.

b) Flows through the pipes and the expansion valves are assumed to be adiabatic, and the pump is also assumed to be adiabatic.

c) The flows of refrigerants into the refrigerating system components are assumed to be steady and the homogeneous two-phase model was used.

d) The pressure variation through condenser and evaporator is considered as a linear function of the distance from the inlet of the component ($P(x) = P_{in} + \frac{x}{L}\Delta P$).

e) For the state of equilibrium (dead state, which sets the maximum theoretical work obtainable when another system in a non-equilibrium state interacts with the environment to the equilibrium), 296 K and 100 kPa were used.

FC-72, with given properties in Table 2.1, was used as the working fluid in the closed-loop system.

Table 2.1. FC-72 properties [37].

Saturation temperature (K)	Liquid density (kg/m^3)	Vapor density (kg/m^3)	Liquid enthalpy (kJ/kg)	Vapor enthalpy (kJ/kg)	Liquid Entropy (KJ/kg.K)	Vapor Entropy (KJ/kg.K)
296	1724.8	3.88	58.48	163.78	0.218	0.563
329	1601.55	13.07	94.76	189.81	0.334	0.616
330	1597.8	13.49	95.88	190.82	0.338	0.619

2.5 Uncertainty analysis

Uncertainty analysis was based on the error propagation of experimental data using the methodology proposed by Coleman et al. [38]. The general formulation is expressed as:

$$U_y = \sqrt{\sum_{i=1}^{n} \left\{ \left(\frac{\partial y}{\partial x_i} \right) . U_{x_i} \right\}^2} \tag{2.14}$$

U_{x_i} is the uncertainty in parameter x_i. The parameters in our experiments with the corresponding uncertainties are listed in Table 2.2.

Table 2.2. Uncertainties in parameters.

Parameters	Uncertainties
Voltage	±1 V
Current	± 0.1 A
Thermocouples	±0.5 °C
Heat flux	±5%
Flow meter	±2%
Pressure	±5%
Heat transfer coefficient	±3%
Coefficient of performance	±3%

3 CHAPTER THREE: Surface modifications and characterization

3.1 Bio-coating

3.1.1 Sulfolobus solfataricus culture

Archaeal cells have a unicellular structure with circular chromosome. They resemble to eukaryotic cells due to their metabolisms involving DNA replication and transcription. However, they remarkably exhibit the same structure and morphology and other macromolecule metabolisms as of prokaryotes [39]. Nevertheless, archaeal domains harbor distinctive complex traits at molecular level that enable them to endure extreme physiological conditions such as low or high temperatures (−2 °C to 15 °C or 60 °C to 122 °C), high salinity (2 M to 5 M NaCl), and low or high pH (<4 or >9) [40],[41],[42]. *Sulfolobus solfataricus* is a hyperthermophilic sulfur metabolizing archaeon, which belongs to Crenarchaeota phylum. This species grows best at temperatures around 80° C and highly acidic pH (2-4). *Sulfolobus solfataricus* essentially metabolizes sulfur as a main cellular metabolism. *Sulfolobus solfataricus* cells generally have a spherical shape processing flagellums, which generate frequent lobes [43]. Highly thermostable properties of this species make it a strong candidate for biotechnological applications regarding heat transfer enhancement.

The initial batch of *Sulfolobus solfataricus* was purchased from American Type Culture Collection (ATCC® 35092™), and the growth medium was prepared according to the ATCC® Medium 1304 recipe. The medium composition is provided in Table 3.1.

Table 3.1. Sulfoloubus solfactricus Medium compositions.

ATCC medium (1304 *Sulfoloubus solfactricus* medium)	**Amount**
Yeast Extract (BD 212750)	1 g
Casamino Acids (BD 223050)	1 g
KH_2PO_4	3.1 g
$(NH_4)_2 SO_4$	2.5 g
$MgSO_4 . 7 H_2O$	0.2 g
$CaCl_2 . 2 H_2O$	0.25 g
$MnCl_2 . 4 H_2O$	1.8 mg
$Na_2B_4O_7 . 10 H_2O$	4.5 mg
$ZnSO_4 . 7 H_2O$	0.22 mg
$CuCl_2 . 2 H_2O$	0.05 mg
$Na_2MoO_4 . 2 H_2O$	0.03 mg
$VOSO_4 . 2 H_2O$	0.03 mg
$CoSO_4 . 7 H_2O$	0.01 mg
Distilled water	1 L

Since *Sulfolobus solfataricus* prefers anaerobic growth, the initial cultivation rate was relatively slow during the preparation. In order to reach maximum growth rate, the culture volume was stepwise increased. Conical flask containing 30mL of pre-warmed medium was first inoculated using aliquot of the cell vial. Then, the cell growth was monitored using UV Spectrophotometer at OD_{600} for 72 - 96h. The culture volume was gradually increased up to 100 mL, 250 mL, and 500 mL by adding pre-warmed medium.

Following the ATCC medium recipe, several adjustments and experiments have been done. Initially, in order to grow the archaea at high speed, its response to growth factor, namely sugar, had to be tested. Therefore, two different batches have been started; one is with sucrose and one is without sucrose. As it has resulted, batch without sucrose has reached OD600: 0.2, and the population has transformed into death phase, gradually died. Accordingly, production of batch with sucrose has been kept going on and the result has been concluded as, sucrose is a fastresponsive growth factor and increases the maximal batch concentration (Figure 3.1). Initial growth stage is critical and in this species, lag phase of bacterial growth stages takes long period of time as 2 weeks. However, many batch cultures have been tested under different conditions and data related to the growth regulation has been collected. Therefore, required properties for the Archaeon have been optimized.

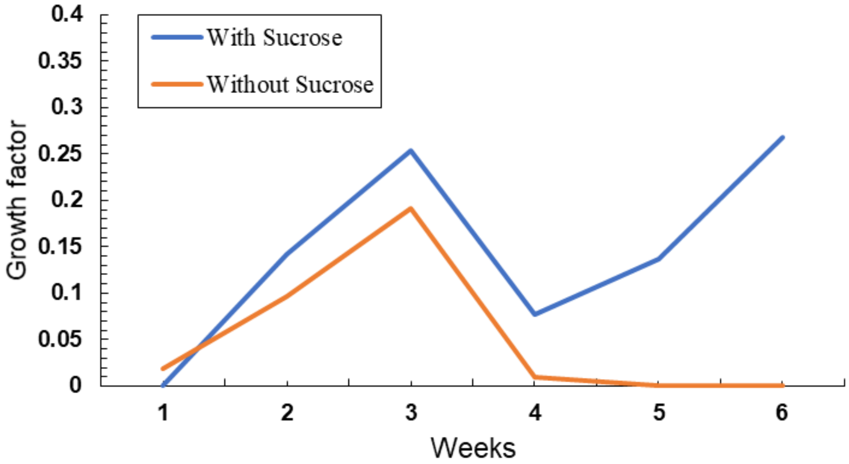

Figure 3.1. Comparison of growth factor. 2g/L of sucrose has been added in the medium. At week 3, 4 and 5, batch volume has been increased, 100 mL, 250 mL and 500 mL, respectively.

Consequently, to generate the mass production of the archaeon in a sustainable manner, the growth medium was supplied with 2 g/L D-sucrose, and the cells were grown at constant temperature and PH of 84°C and 3.9, respectively. When the OD_{600} of culture reached to 1, 250 ml of the culture was harvested after cooling down on ice and further harvested using centrifugation at 4500 ×g for 15 min. The remaining culture was added with the fresh medium up to 500 ml and was kept for further incubation. Then, the supernatant was discarded, and the pellet was stored at −80 °C until use.

In order to prepare bio-coated surfaces, the pellet was washed once with 250ml of phosphate buffer (20% (v/v) in H_20) at room temperature and then re-suspended with 250ml of fresh phosphate buffer. Finally, Poly-L-lysine (0.1 % (w/v) in H_2O) was added into the suspension with a ratio of 1:5 to increase the adhesion of the biomaterial to the desired surface. Then, the coating mixture was applied on the silicon wafer with thickness of 500µm and interior side of an evaporator made of aluminum. Subsequently, the coated samples were incubated at room temperature as well as at 60°C to initiate the evaporation process. Figure 3.2 summarizes the culture, coating and drying processes. More information about the coating process of the aluminum tube is provided in section 3.1.3.

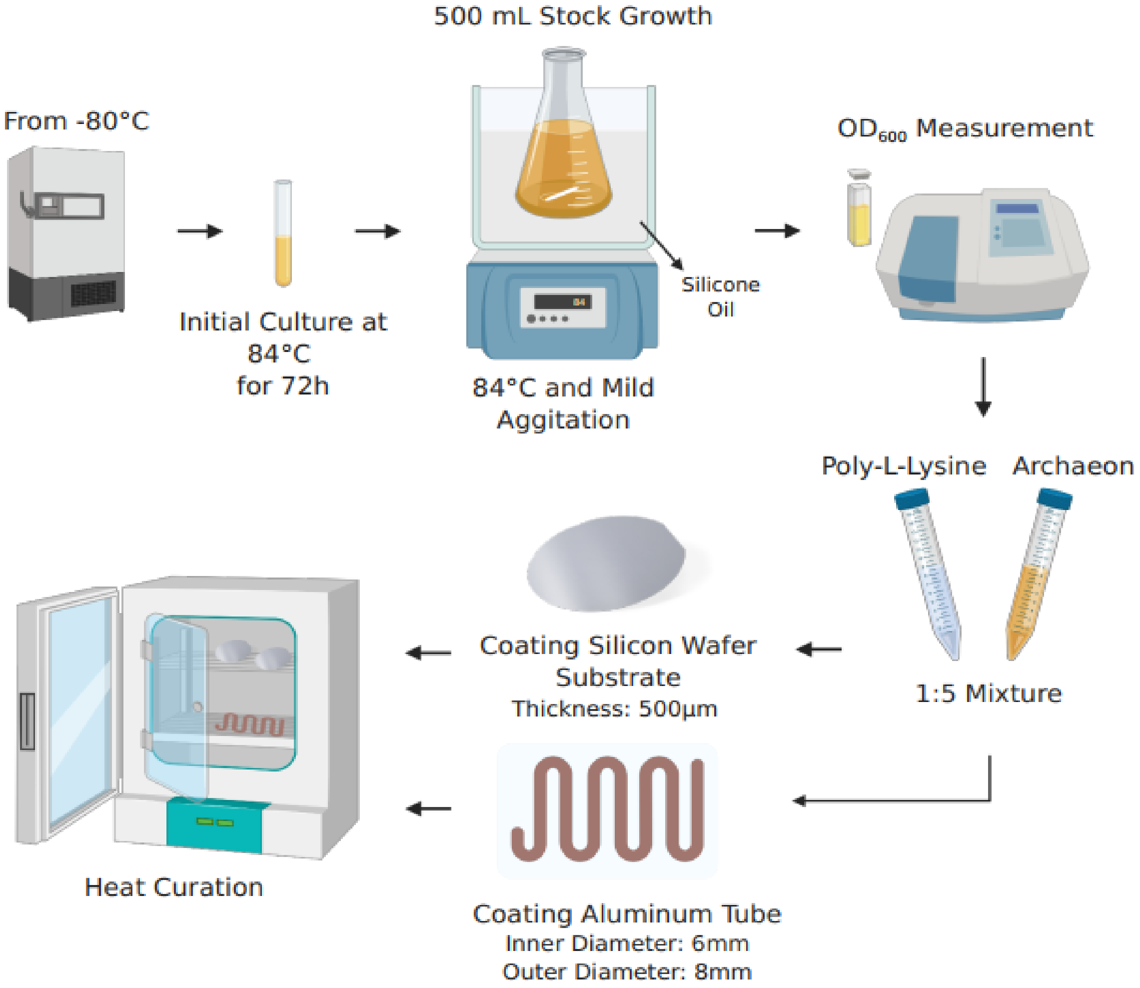

Figure 3.2. Culturing, coating and drying processes of *Sulfolobus Solfataricus*.

3.1.2 Optimization process of the biocoating

Several factors have been considered during the coating process. First of all, supernatant and pellet parts of the centrifuged Archaea suspension were investigated to study the effect of concentration on surface morphology. As it can be seen in Figure 3.3, pellet part of the suspension give higher valleys and peaks to the coating. It should be noted that two different batches were cultured and coated to see the effect of culture on biocoating.

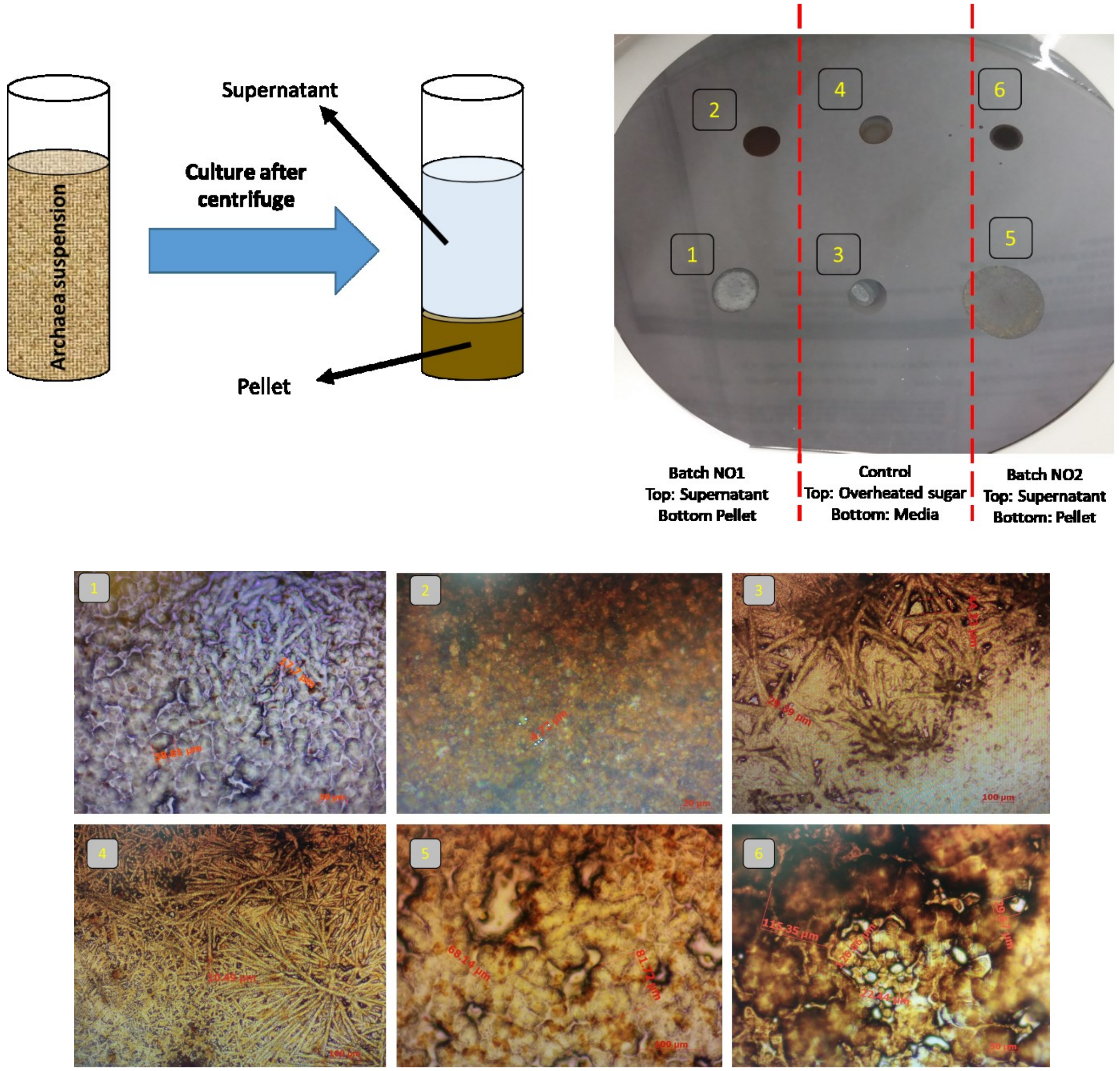

Figure 3.3. Surface morphologies during the optimization process.

3.1.3 Coating process of the aluminum tube

A lab-made long oven was prepared to dry the coated long tube while rotating. The drying system is shown in Figure 3.4. The air was blown by air compressor to the heat chamber and the temperature of the air was increased to 300°C. The heating part has a resistance in a lamp, which acquires power from the power supply. It passes into five paths to dry the pipe in five regions of the oven. The pipe has 6 ball bearings to keep the pipe straight during the rotation. The inner volume of this 2 meter long tube is about 60 ml and the archaea's mixture volume injected to the tube is about 40 ml to allow the fluid to evaporate better during the rotation. After being sure that the inside of the tube was coated and it was dry, the 2 meter long tube was bent by the Swagelok tube bender to make the evaporator.

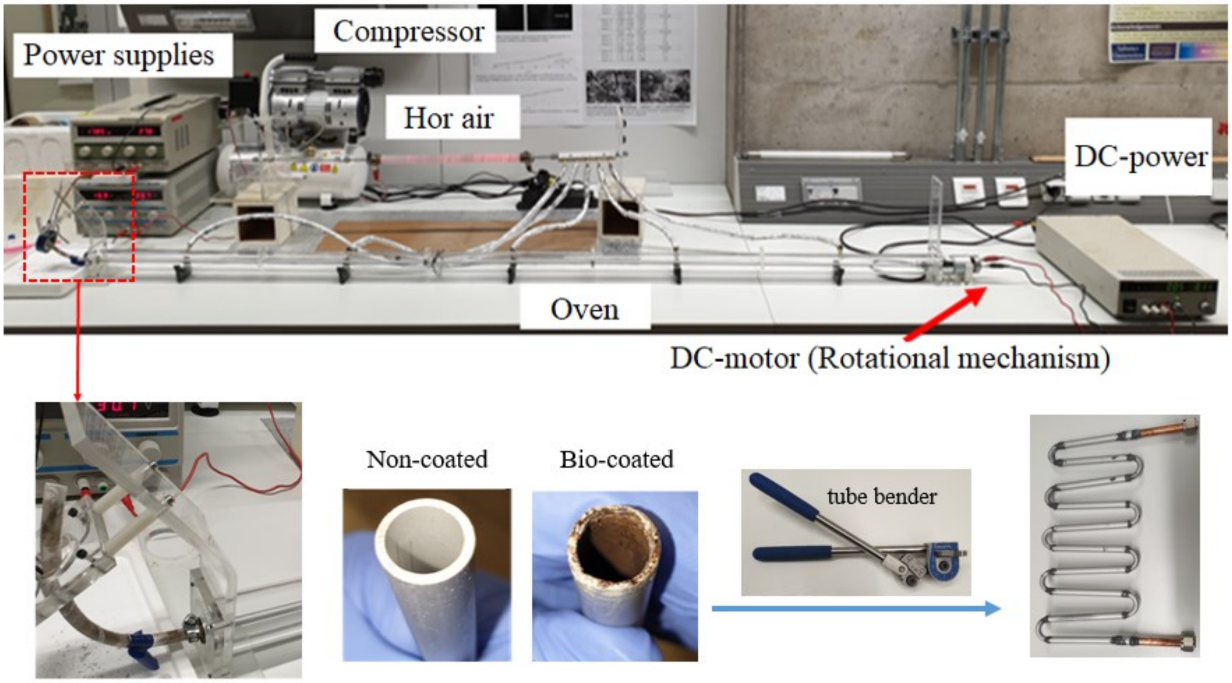

Figure 3.4. The coating procedure of the aluminum tube.

3.1.4 Surface characterization on silicon substrate

Once coated surfaces were completely dried, they were processed for the surface characterization. To avoid disparity, which might generate as a result of surface charge formation of biomaterial, and to develop homogeneous surface for high resolution image processing, a thin layer (3-4 nm) of gold-palladium alloy was employed using SEM sputter coater. A scanning electron microscope (SEM Leo Supra 35VP, Oberkochen, Germany) was used to capture the microscale images of the coated samples. The Secondary Electrons (SE) mode was used for the imaging due to its high spatial resolution. The images were taken using the SE mode at low voltage (3KV and 10KV) in 0 and 45 degree titled visions to obtain both full images of the surface area and the cross sectional area. The wettability of the bio-coated surfaces was measured using the water contact angle (WCA) method [44]. A 5µL of the water drop was applied on the five various spots of each sample, and their relevant average contact angle was determined.

Surface characterization using AFM (Atomic Force Microscopy) indicated that the average thickness in porous and roughened surfaces was 1.2 µm. The drying time of the samples incubated at room temperature was 30 hours, whereas the drying time of the specimens incubated in the oven at 60°C was 1.5 hours.

Figure 3.5a shows the *Sulfolobus Solfataricus* cells fixed on the substrate surface (using 2.5% glutaraldehyde dissolved in phosphate-buffered saline (PBS) and kept at the room temperature for drying). The resulting electron microscopy image of the highly diluted single cell sample that lacks fixation solution is shown in Figure 3.5b. This sample was dried under the freeze-drying condition for 2 hours. This figure shows that the morphology of the cell remained intact, while the interior fluid material was completely dried as a result of the ice sublimation and formed the porous structure. Figure 3.6a and Figure 3.6b demonstrate the dried bio-coating (concentrated cells with poly-l-lysine) on silicon substrates under different drying conditions.

In addition to silicon surfaces, the bio-coatings were prepared and characterized on metallic surfaces including copper, aluminum and stainless-steel (Figure 3.11). Similar to silicon and glass substrates, metallic surfaces also have rough and porous morphologies under dip coating conditions.

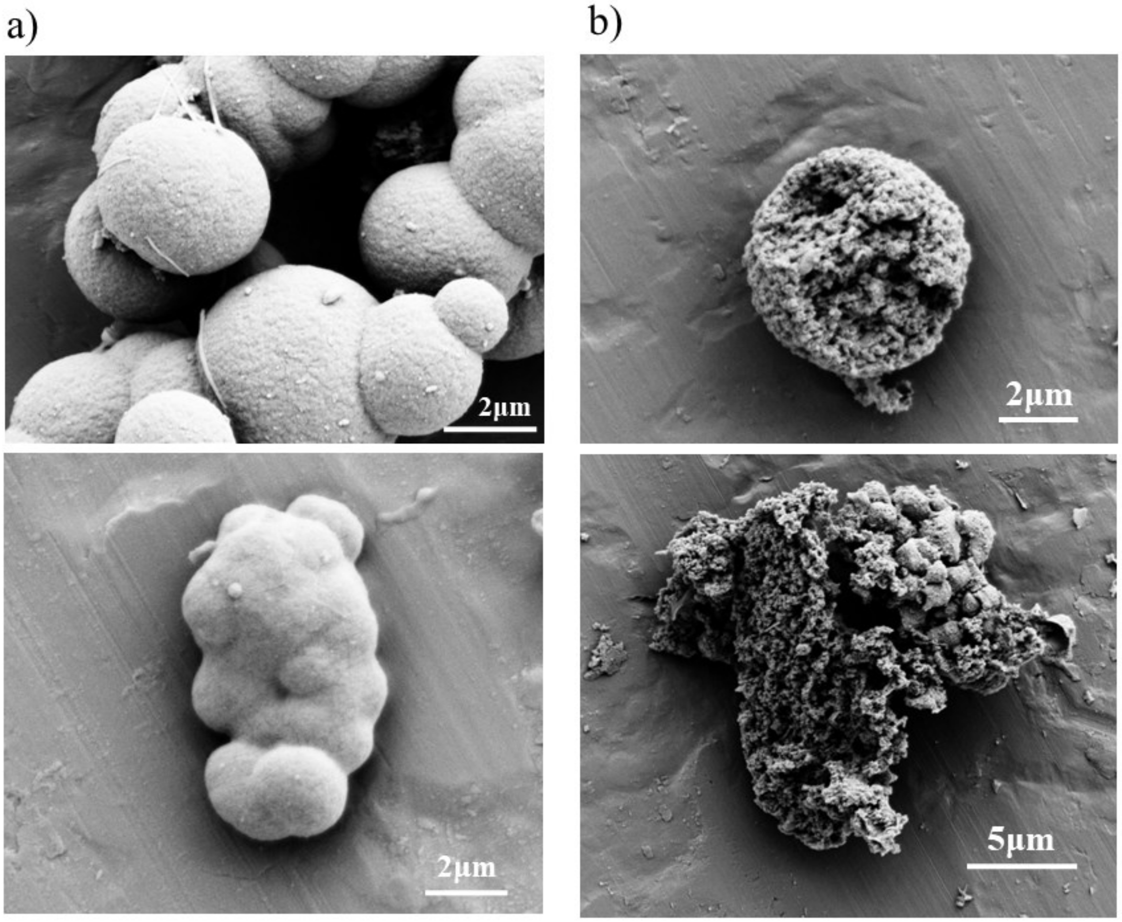

Figure 3.5. a) S.Solfataricus fixed cells in a highly diluted sample. b) Porous structure inside a single cell of S. Solfataricus in a highly diluted sample and merged interior parts of some cells.

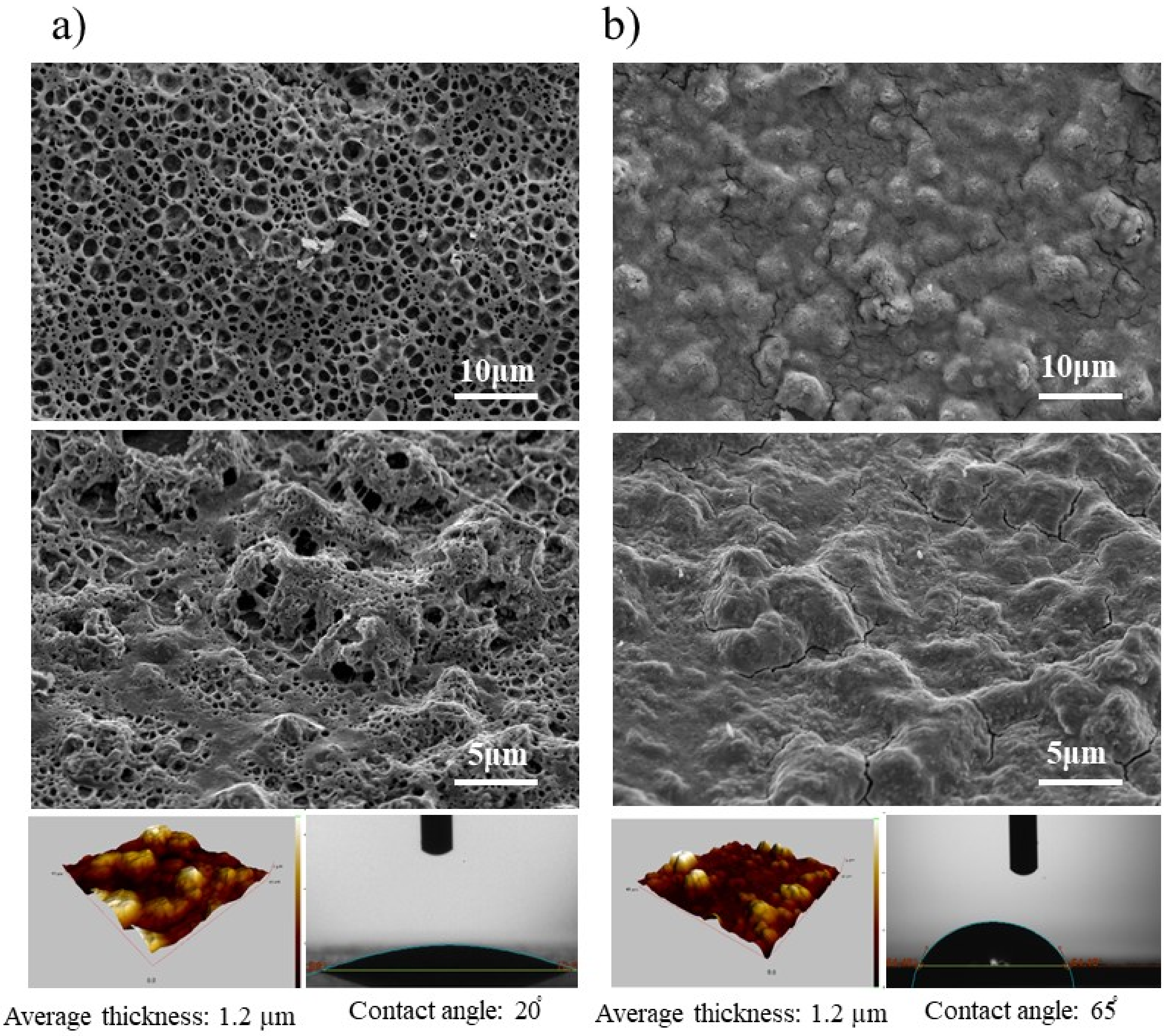

Figure 3.6. 2D and 3D SEM images of the bio-coated silicon substrates, AFM results and contact angles of the samples under two different drying conditions: a) Porous surface achieved at 60°C heat incubation, b) Roughened surface achieved after drying at room temperature.

3.1.5 Micro-porous and micro-roughness as a result of bio-film morphology alteration

The bio-coating surface is inspired by microbial biofilm formation. Generally, the biofilm formation is considered as a significant survival mechanism in microbial life, which protects the microorganism from austere conditions such as nutrient scarcity, unfavorable temperature or acidic condition. Archaeal cells possess several survival strategy to adapt with various harsh condition.

For example, to balance the pH of the cells' interior with outside acidic condition (pH <3), they have developed a mechanism to synthesis a thicker layer of the sugar coated shelter. This cell's coating comprises of tetraether structure of lipids membranes on outside of the cell membrane to resist the proton invasion in acidic environment of the outside growing medium to protect the nutria pH of inside cells [45].

Similar to bacterial cells, archaeal cells form biofilm, where cells initiate the self-immobilization and build up the stacked layers to adapt to the temporary mutual lifestyle. In the biofilm process, cells inevitably produce multilayer microbial community, which leads to irreversible attachment, subsequent development of micro colonies and a further process for the biofilm maturation. In response to various stress states, death signals induce autolysis of some microbes to provide nutrition for colony survival known as "die for community" [46].

The proposed bio-coating process employs *Sulfolobus Solfataricus* to form a biofilm on the surface using poly-l-lysine to act as an extracellular polymeric substance (EPS). The structure of the bio-coated layer developed under the room temperature displays roughness mainly due to smooth autolysis of the surface microbial biofilm. However, the porous shape structures form due to the rapid release of the gasses such as H_2S, CO_2 and SO_2, which consequently generate a distinct morphological structure on the biofilm (Figure 3.7). These porous structures identified as micro and nano structures reflect the trace of the released gasses and demolished cells. In addition, the rapid evaporation withdraws more dissolved gases to the bio-layer/air interface and aligns the micro-organisms in dispersed fashion and thus establishes the porous structure. On the other hand, evaporation at room temperature corresponding to the steady state form of evaporation allows micro-organisms to slowly descend on the substrate and forms the roughened coating.

Most of the Sulfolobus species display aerobic growth. However, *Sulfolobus Solfataricus* has a higher growth rate at low oxygen concentrations [47]. Aerobic microorganisms grow in the presence of the oxygen when the O is the final electron acceptor, and water and CO_2 are the final products. Additionally, Sulfolobus species are known to be chemosynthesis microorganisms due to their ability in oxidizing sulfur to metabolize various carbon sources and consequently direct the energy for carbon fixation. Our carbon source to grow *Sulfolobus Solfataricus* is D-sucrose. Sucrose is a disaccharide consisting of glucose and fructose. Aerobic metabolism generates CO_2 as a result of the glucose oxidation. Basically, they gain energy from growing on sulfur or various organic compounds. Sulfur metabolism pathways in archaea are part of the food chain survival strategy, when there is a lack of energy source, sunlight, nearby hydrothermal vents, with abundant hydrogen sulfide and carbon dioxide. The SO_4^{2-} is the prerequisite in sulfur metabolism pathway of *Sulfolobus Solfataricus,* which produces H_2S gas through three sequential reactions [48] as indicated in Figure 3.7. Moreover, these microorganisms could metabolize organic sulfur and emit H_2S under aerobic conditions [49]. It was reported that in some studies the rate of oxidation is determined by the biogeochemical characteristics of the sediment in sulfur-oxidizing microorganisms [50],[51]. According to these studies, the rate of the sulfur oxidation in such microbes is more on the sediment surface, where enormous amount of the oxidants is available as a result of high rate sulfur reduction [52]. Most of the sulfide oxidizing microorganisms grown in lab cultures are mostly derived from surface sediments [53].

Temperature discrepancy between two samples is the main reason to generate various morphologies defined as roughness and porous coatings. This temperature difference has two main effects on the evaporation rate and resulting cell sedimentation: i) Surface evaporation occurs as a result of vapor transport at the bio-film/air interface. The vapor transport is highly dependent on the diffusion coefficient of the dissolved gas, where the diffusion coefficient exponentially increases with the temperature [54]. For example, the diffusion coefficient of air is almost five times higher at 60°C compared to the room temperature. ii) The second reason is derived from the differences in solubility of the generated gases within the biomaterial at different temperatures. At higher temperatures, the solubility of the generated gases such as H_2S, SO_2, CO_2 and air decreases exponentially and results in major difference in gas release from the bio-film (Table 3.2). This rapid release of the gasses at 60°C contributes to the alteration in sedimentation profile and also the bio-film rupture.

Table 3.2. Solubility of the gases in water (g gas per kg water) [55].

Gases in the biomaterial	At 20°C	At 60°C	Percentage of reduction
CO_2	1.7	0.6	64.7%
H_2S	3.85	1.5	61%
SO_2	115	45	60.8%
Air	0.024	0.013	45.8%

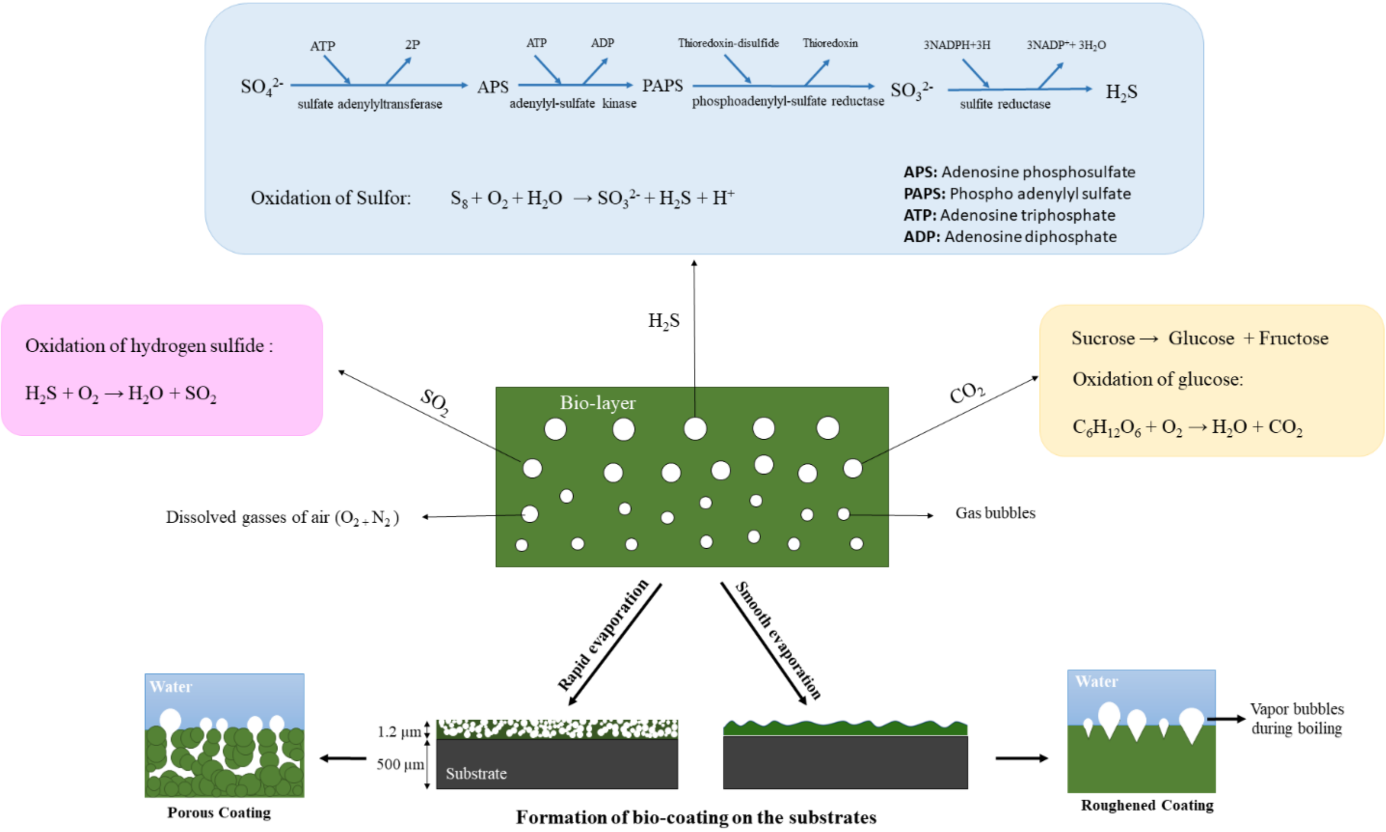

Figure 3.7. Generation of CO2, H2S and SO2 as a result of Sulfolobus sulfactorius biological metabolism [39]. Figure depicting evaporation of bio-layer under two different conditions (rapid and smooth). The rapid evaporation results in formation of the porous structure, whereas smooth evaporation causes roughened bio-film on the substrate. The schematics represent two various bio-coated morphological surfaces and their function once boiling occurs.

3.1.6 Numerical simulation and force analysis of rising gas bubbles during evaporation

During evaporation, the evaporation momentum force (F_E), viscous force (F_V) and Buoyancy force (F_B) are on the generated gas bubbles (Figure 3.8) inside the wet bio-layer, have a major effect on the shape of the moving gases inside the layer.

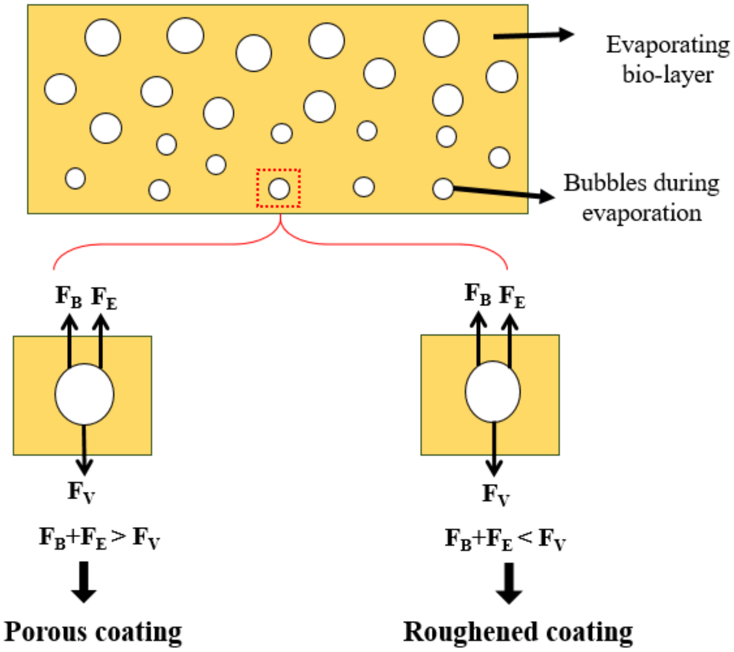

Figure 3.8. Force analysis on the rising gas bubbles during evaporation of the bio-layer.

$$F_E = \left(\frac{q^{"}}{h_{fg}}\right)^2 \frac{1}{\rho_g} H \tag{3.1}$$

$$F_B = mg \frac{\rho_L}{\rho_g} \tag{3.2}$$

$$F_V = 6\pi r \eta u \tag{3.3}$$

$$F_E + F_V + F_B = 0 \tag{3.4}$$

Where $q^{"}$ is the interfacial heat flux, h_{fg} is the latent heat of vaporization, ρ_g is the vapor density and H is the cross-sectional height of the bubble. m is the mass of the bubble and ρ_L is the density of the liquid. r is the radius of the bubble, η is the dynamic viscosity of the liquid and u is the velocity of the ascending bubble.

According to the applied mentioned forces on the rising bubbles, the effect of dynamic viscosity, bubble diameter and heat fluxes during evaporation are analyzed by the numerical simulation results (Figure 3.9). Numerical analysis on the rising bubbles during evaporation were carried out using level set method in COMSOL Multiphysics 5.4.

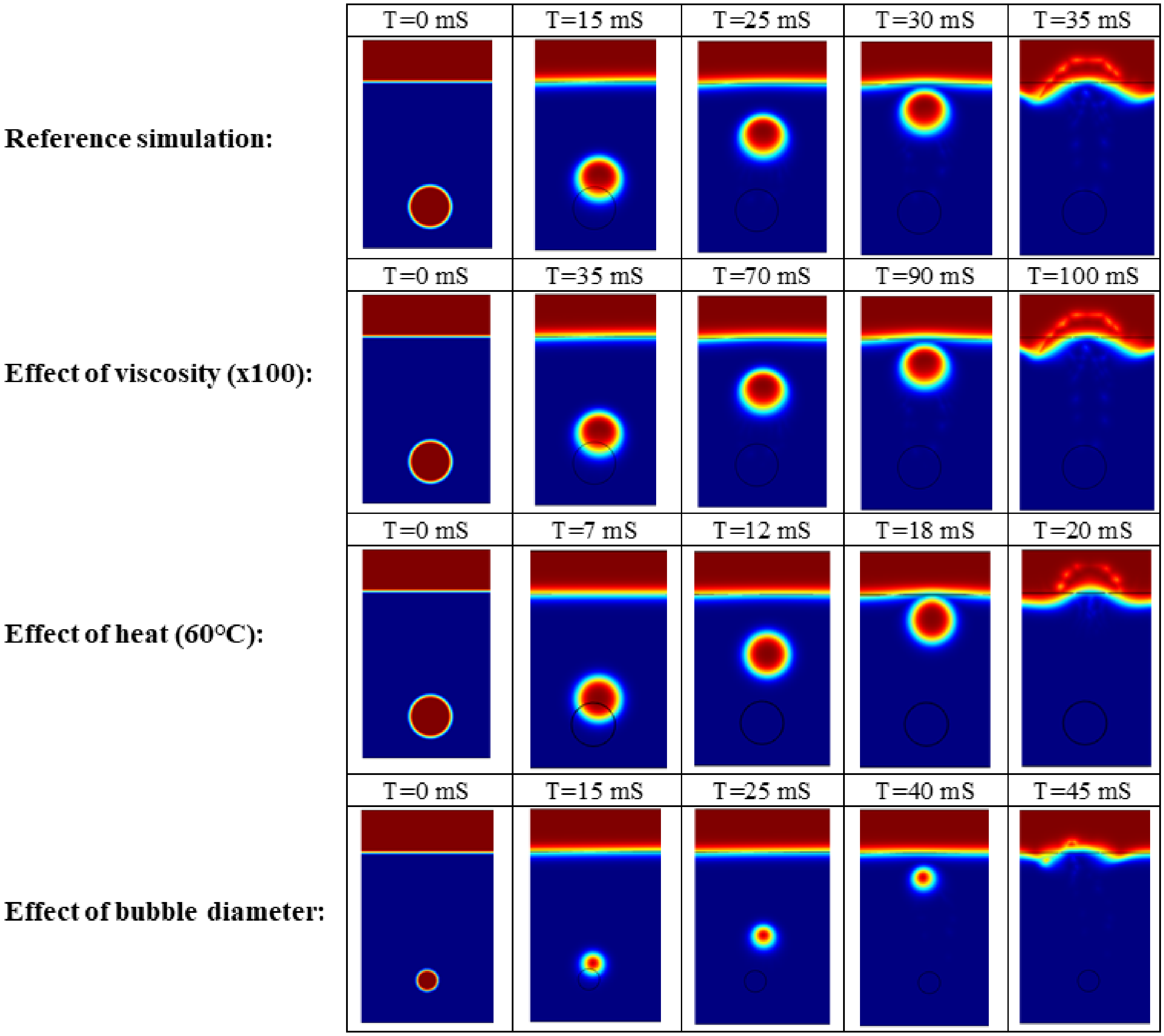

Figure 3.9. Numerical simulation on the effect of viscosity, heat and bubble diameter on rising gas bubble during evaporation.

Increasing dynamic viscosity in other constant conditions, would delay the bubble departure, which satisfy the existence of the viscous force to the downward on the rising bubble. In addition, bubble diameter would influence on the both evaporation force and viscous force but its effect is more dominant in the viscous force. Applying heat as the initial condition would directly increase the evaporation force in the upward direction. A dominant viscous over evaporation force results in the bubble trapping inside the wet bio-layer. However, under free convention condition at the room temperature, surface evaporation occurred gradually and all the emerging bubbles came up to the surface. Here the bubbles collapse smoothly at the air/bio-layer interface and create the roughened morphology. Also as stated in section 3.1.5, by applying heat, rising gas bubbles are inclined to depart from the bio-layer rapidly that leads to biofilm destruction. Numerical simulation shows that rising bubbles are merged to each other when they are ascending and that is the reason behind the inter-connected micron-size channels after drying (Figure 3.10).

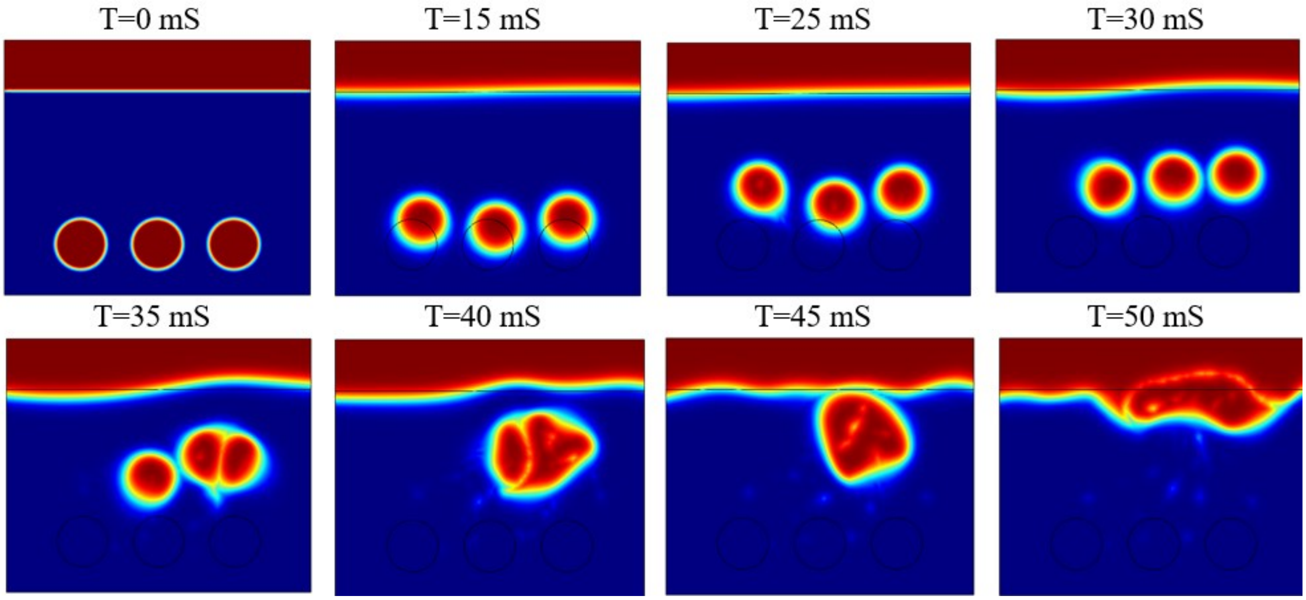

Figure 3.10. Numerical simulation of multiple rising gas bubbles during evaporation that results in inter-connected porous structures.

3.1.7 Metallic bio-coated surfaces

SEM (Scanning Electron Microscopy) images of the bio-coatings on top of the polished metallic substrates such as stainless steel, aluminum and copper are depicted in Figure 3.11. It should be noted that all of the substrates are fully polished before coating using sandpapers.

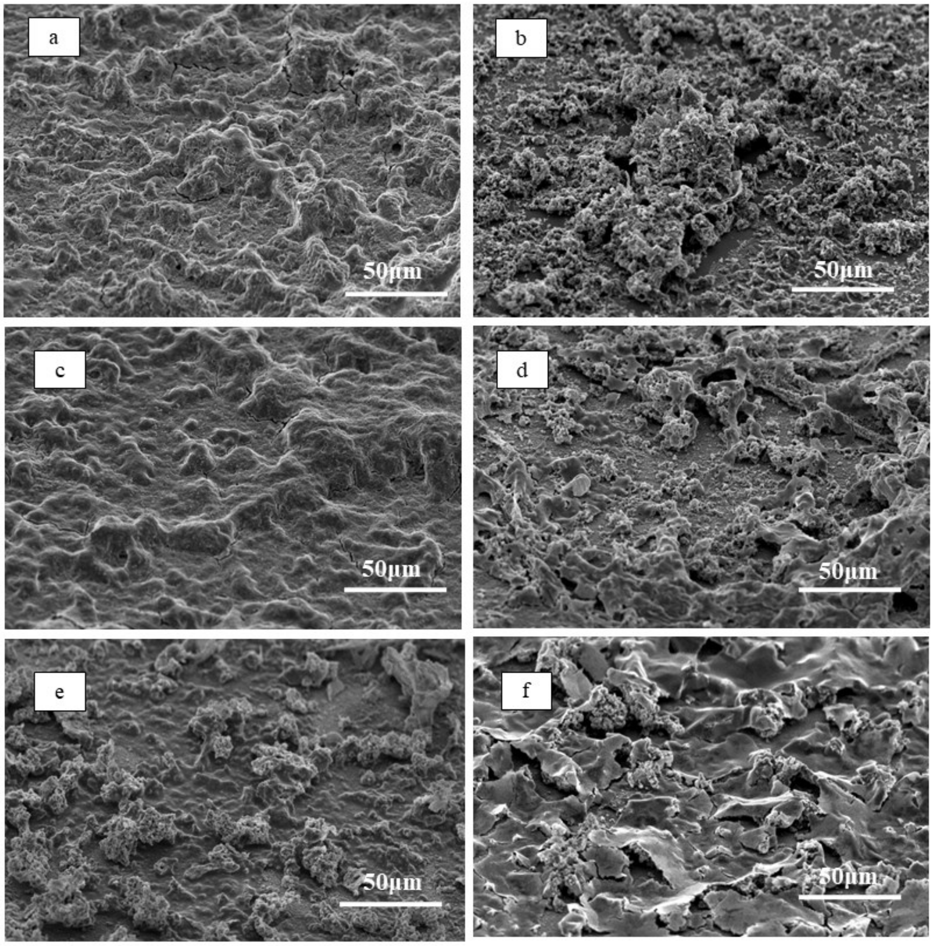

Figure 3.11. SEM images of the surface morphologies on different metallic substrates: a) roughness coating on stainless steel, b) porous coating on stainless steel, c) roughness coating on aluminum, d) porous coating on aluminum, e) roughness coating on copper, f) porous coating on copper.

3.2 Combination of artificial roughness and bio-coating

Since coatings are considered as an external surface modifications technique, surface treatment before coating is of great importance. Surface treatment on silicon substrates requires expensive facilities such as RIE or DRIE machines, whereas, surface treatment can be applied easily on metallic surfaces such as aluminum and copper via sandpapers. For investigating the effect of surface roughness, copper and aluminum plates were diced into square shapes 15mm×15mm fitted to pool boiling experimental setup. Then the squares were grinded with different sandpapers (grit size 400 to 3000) via the Gripto #2 device shown in Figure 3.12. It should be noted that the sand paper with grit size of 3000 was used to make the surfaces fully polished. The samples were washed continuously for cleaning the grinded particles from the substrate's surface. After grinding and polishing, the samples were cleaned by immersion into Acetone, IPA (Isopropyl alcohol) and DI water respectively. All of the cleaning processes were took place in the sonication bath for better efficiency. After cleaning process, they were immediately dried using Nitrogen gun to remove any droplet from the surface in order to prevent oxidation. Then the samples were placed in the heat resistant 3D-printed walls for pouring bio-coating material on them using dip-coating method. Then the samples were kept in the oven at 60°C for applying porous bio-coating structures on top of the artificial sanded roughness.

Figure 3.12. Grinding and polishing the metallic surface before applying bio-coating on them.

4 CHAPTER FOUR: RESULTS AND DISCUSSION

4.1 Heat transfer performance of bio-coated silicon surfaces in flow boiling setup

Pool boiling experiments on the porous bio-coating with two different thickness were performed previously by our team [56]. Here, flow boiling experiments are conducted on porous and rough bio-coated silicons to investigate boiling heat transfer of the mentioned surfaces in a minichannel for the purpose of electronic cooling. Figure 4.1a clearly reveals that the porous-coated surface has higher CHF values compared to other surfaces. Furthermore, higher CHF values were obtained at lower wall superheat, which suggests lower surface temperatures for the porous-coated samples. The main reason for enhancements is the interconnected pore networks, which enhance the liquid wetting and vapor venting at higher heat fluxes (shown in Figure 4.1b). Accordingly, enhancements of 11%, 20.7%, 74.5%, 94.1% and 76.3% are achieved at 10 (W/cm^2), 20 (W/cm^2), 40 (W/cm^2), 60 (W/cm^2), and 80 (W/cm^2) heat fluxes, respectively.

The obtained results for rough-coated surfaces also prove enhancements in HTC and CHF. The roughened surface provides abundant nucleation site densities, and the performance of this surface appears to be better at lower heat fluxes, while its function gradually deteriorates at higher heat fluxes. Enhancements of 22%, 35.6%, 25.7%, 15.7% and 10.7% are obtained at 10 (W/cm^2), 20 (W/cm^2), 40 (W/cm^2), 60 (W/cm^2), and 80 (W/cm^2) heat fluxes, respectively. As can be seen, compared to other samples, rough surfaces have a better cooling performance at low wall superheats (ΔT_{sat}<15K). At this range of wall superheats, the rough-coating offers smaller bubbles compared to the porous-coated surface, which is a result of abundant nucleation sites provided by this type of coating. The visualization studies at the applied heat flux of 20 W/cm^2 indicate that the bio-coated samples resulted in the formation of more bubbles and heat transfer enhancement (Figure 4.1b).

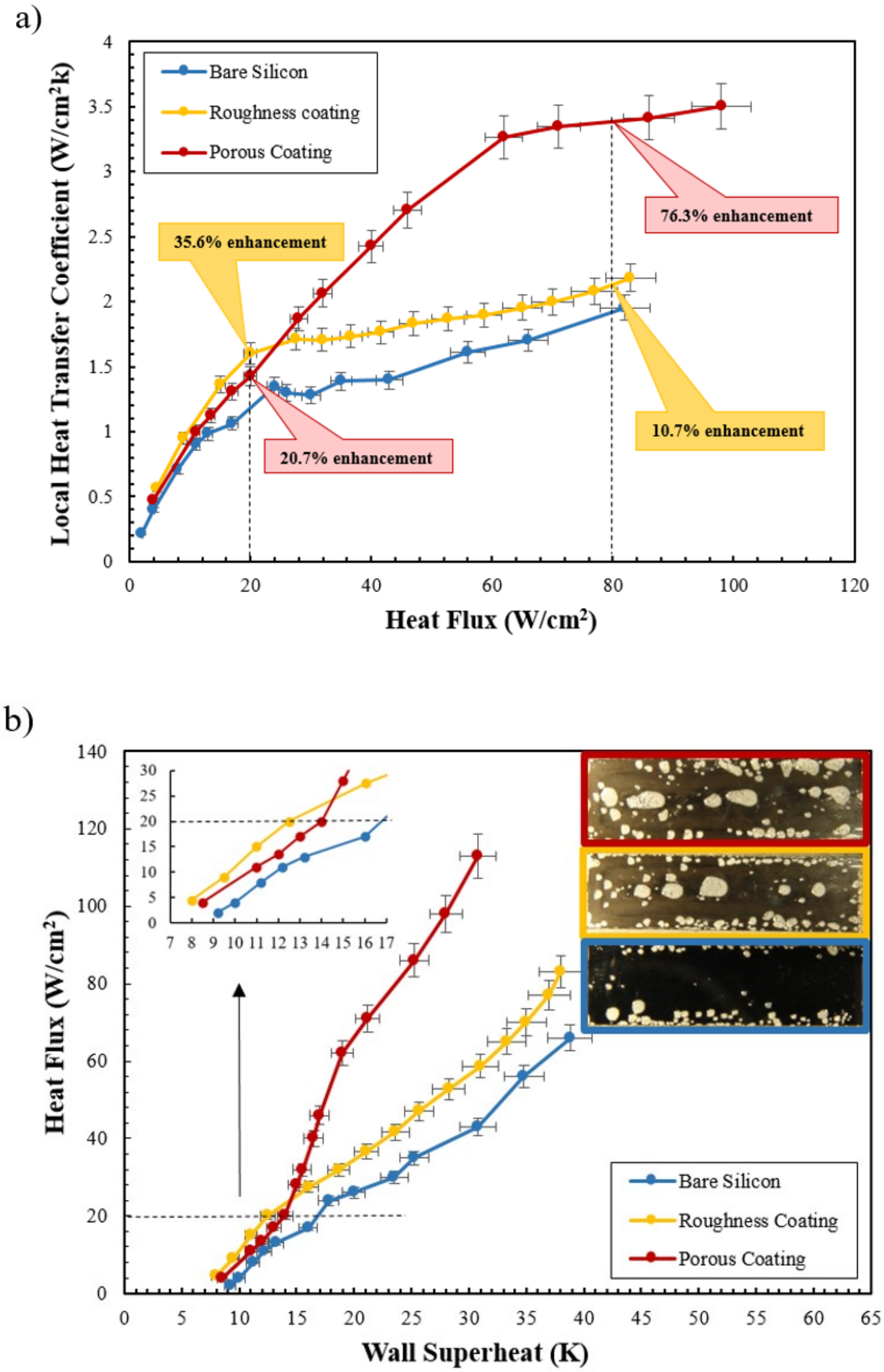

Figure 4.1. The effect of roughened and porous bio-coated surfaces on boiling heat transfer at the mass flux of 100 kg/m^{2}s. a) Local heat transfer coefficient profile and enhancements for nucleate boiling regime and near CHF, b) Wall superheat-heat flux profile and boiling images of the non-coated and bio-coated surfaces at nucleate boiling regime for the heat flux of 20 W/cm^2.

4.2 Visualization studies on flow boiling experiments

Visualization studies were performed on the bio-coated and non-coated surfaces. The visualization results on the rough-coated surface clearly indicate the generation of tiny bubbles (marked in yellow in Figure 4.2a). This is due to presence of abundant nucleation sites on the rough-coated surfaces. However, on the non-coated surfaces, many slugs (large vapor bubbles) can be observed. These slugs prevent the surface rewetting path and results in a high surface temperature beneath the large vapor bubbles. On the other hand, on the rough-coated surface, these tiny bubbles move towards the surface, thereby rewetting the surface and increasing the cooling efficiency of the surface (marked in red in Figure 4.2a) [57].

On the porous-coated surfaces, as a result of the presence of many interconnected channels (as shown in SEM images in Figure 3.6 a), transportation of coolant within the bio-coating takes place during the boiling process, especially at higher heat fluxes. These interconnected channels act as liquid supply paths when large vapor blankets form at high temperatures. As a result of this effect, the flow morphology (distribution of vapor phase inside the two-phase flow) changes dramatically. As can be seen in Figure 4.2b, compared to the non-coated surface, the porous-coated surface houses a more distributed vapor phase, which is more evident at high heat fluxes ($q \geq 40$ W/cm^2).

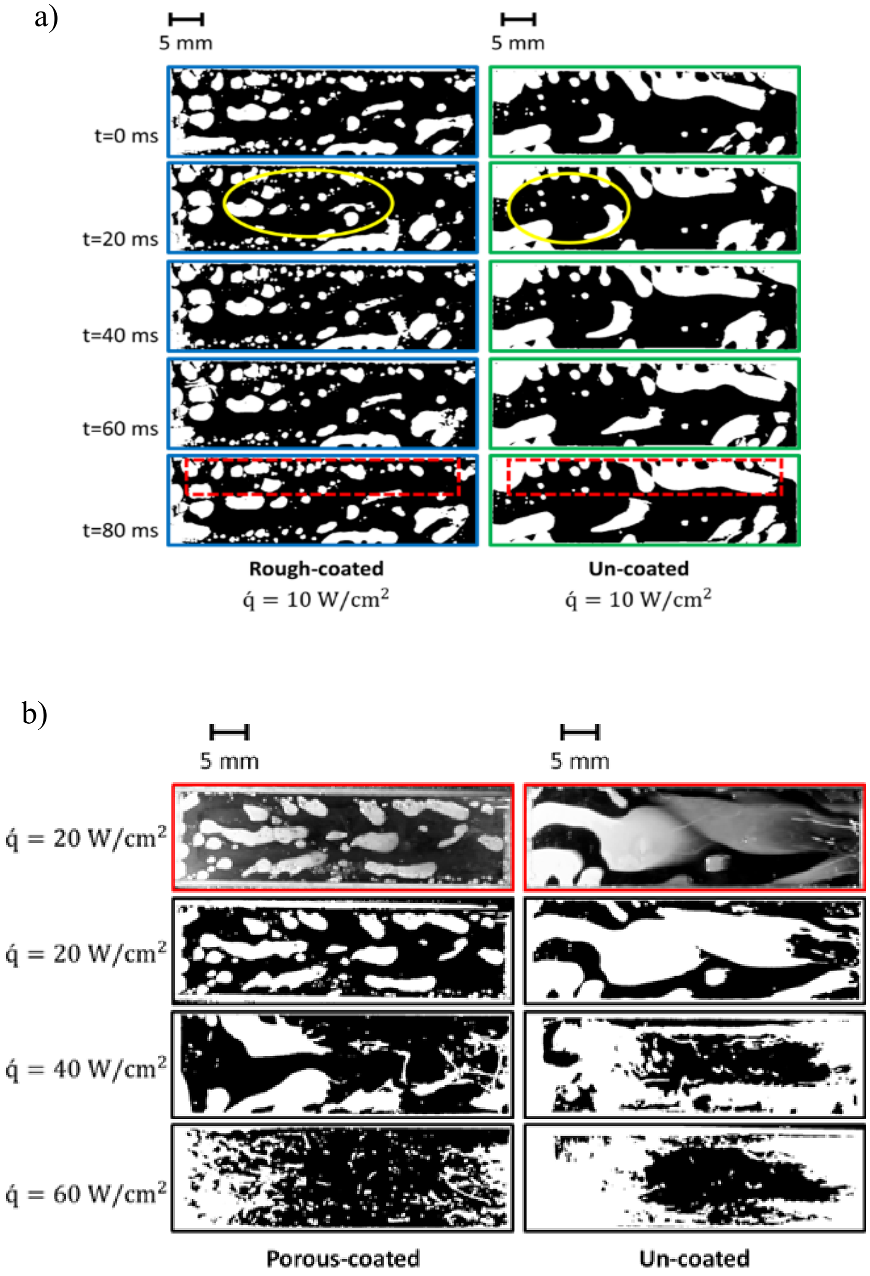

Figure 4.2. Boiling experiments visualization. a) Rough-coated surface at constant heat flux, b) porous-coated surface at different heat fluxes. Here, liquid and vapor phases are shown in black and white colors, respectively.

4.3 Lab-made AC system performance analysis

Based on the obtained promising results from the boiling experiments, a miniature air conditioning system was assembled to examine the performance of the bio-coated evaporators. First and second laws of thermodynamic are used to analyze the performance of the system. In the energy analysis, when the first law of thermodynamics is considered, all types of energy are taken into account and the quality of energy types is neglected. For instance, it is not possible to show the change in the quality of thermal energy from the hot ambient air (heat source) to the evaporator surface (cold source). On the other hand, the exergy analysis involving the second law of thermodynamics leads to a better understanding about the energy transfer process. Basically, the exergy of the system represents the maximum amount of the work when the system comes back to its equilibrium with the environment. This is especially important for cooling applications, where the system will have a waiting period for the next cooling cycle.

4.3.1 Energy analysis, first law analysis

For the air conditioning system, the energy efficiencies of the bio-coated evaporators were investigated by comparing the power consumption of the electrical heaters for bio-coated and non-coated surface evaporators. Each test lasted for an hour, and the average of power consumption was eventually calculated for each sample. The experiments were performed at four different chamber temperatures of 56.5°C, 58.5°C, 61°C and 66°C temperatures (corresponding to 0.5K, 2.5K, 5K and 10K wall superheats, respectively). While the chamber temperature was raised by the heater fan, the evaporator reduced its temperature by absorbing the chamber heat. The PID system deactivated and activated the heater when the temperature of the chamber was higher and lower than the regulated temperature, respectively

Figure 4.3a shows the obtained results for the bio-coated and non-coated surface evaporators under experimental conditions. The obtained results indicate that the modified evaporators have higher cooling capacities compared to the non-coated surface specimen. Here, the cooling power is the amount of absorbed heat to keep the chamber at the desired constant temperatures. The wall superheat in the miniature evaporator is defined as the temperature difference between the chamber temperature and the temperature of the fluid before entering the evaporator. On the other hand, the pressure drops for different components of the setup were obtained and compared. Accordingly, the obtained pressure drops for bio-coated evaporators are almost the same as for the non-coated surface evaporator (only ~3% higher). Coefficient of Performance (COP) was used to evaluate the performance of the system. COP was calculated as:

$$COP_{cooling} = \frac{Q_c}{W} \tag{4.1}$$

In Equation 4.1, Q_c is the heat removed from the heat source (electrical fan) and W is the consumed work by the system. The consumed work is the sum of pumping power, preheater power and chiller power. Related information about the energy consumption of the system components is given in section 2.4.2. Compared to the Non-coated evaporator, the porous-coated evaporator results in enhancements of 0.41%, 1.15%, 6.33% and 11.11%, while the rough-coated evaporator leads to enhancements of 1.66%, 4.38%, 4.66% and 4.44% in cooling COP for chamber at air temperatures of 56.5°C, 58.5°C, 61°C and 66°C, respectively. The obtained results imply a considerable reduction in energy consumption for thermal-fluids applications.

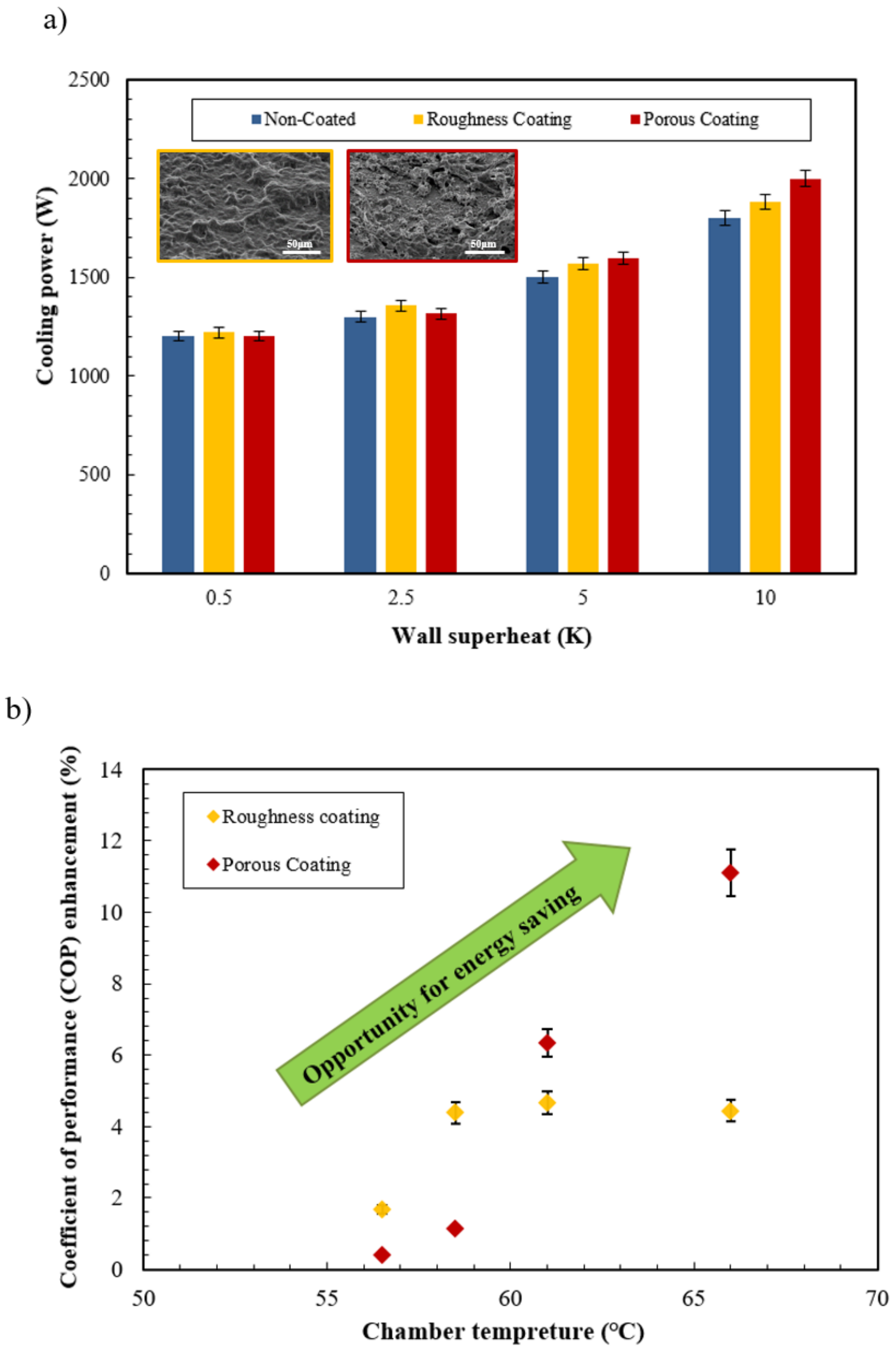

Figure 4.3. a) Obtained cooling power for bio-coated and non-coated surface evaporators at different wall superheats and the SEM images of the bio-coated aluminum surfaces. b) Obtained enhancements in COP for the rough and porous coatings at different chamber temperatures.

According to the obtained results, it can be concluded that the proposed coating has the potential to be used in different applications. Rough-coated refrigerator shows higher enhancement at low wall superheats ($\Delta T<2.5K$) compared to porous-coating, which agrees with the obtained results from fundamental studies. This kind of coating is suitable for small-scale refrigerators with low cooling capacities. On the other hand, porous coating offering a superior COP enhancement at medium and high wall superheats is suitable for larger refrigerators with high cooling capacities.

4.3.2 Exergy analysis, second law

In this section, the second law analysis is presented to give more insight into the energy recovery (exergy availability) for non-coated and coated evaporators. Exergy destruction permits the evaluation of exergy destroyed per component. The quality of the vapor was obtained using a transparent channel at the outlet of the evaporator, and the images was post-processed using ImageJ software.

The first law analysis highlights that the rough- and porous-coated evaporators work more efficiently at low and high temperatures, respectively. Thus, the exergy analysis was performed on rough- and porous-coated surface at wall superheats of 0.5 K and 5 K, respectively. The Second Law analysis is an additional approach for the analysis of heat exchanging devices and allows to evaluate the energy flow between the evaporator surface and the coolant, combining heat transfer and friction effects [58],[59]. Vapor qualities, cooling powers, COPs, evaporator, and total systems exergy destruction rates are tabulated in Table 4.1.

According to the obtained results, the bio-coated evaporator has a lower destruction rate compared to the non-coated case, which is mainly due to enhanced boiling heat transfer capabilities on the proposed coating. The 7.5% and 8.2% enhancements in exergy destruction rates in the evaporator are obtained at 0.5 K and 5 K wall superheats, respectively. As a result, 1.9% and 3.7%

total enhancements are achieved for 0.5 K and 5 K wall superheats. The main reason for the lower total exergy enhancement rates is the high exergy destruction rate in the condenser. The high exergy destruction rate in the condenser is attributed to several factors: i) high temperature difference between inlet and outlet (~35 K), ii) high condensate flow rate (~150 ml/s), iii) the type of the condenser (shell and coil). It should be noted that the aim of this study is to propose an effective coating for the evaporators with the use of the 1st and 2nd laws of thermodynamics. The working conditions for the condenser are not optimized in this study, which will be investigated in the near future by the authors.

Table 4.1. Conditions of the exergy analysis.

Wall superheat (K)	Evaporator type	Vapor Quality(x)	Cooling power (W)	Coefficient of Performance (enhancement)	Evaporator Exergy destruction (W) (enhancement)	Total Exergy destruction (W) (enhancement)
0.5	Non-coated	0	1195	3.428	21.53	45.7
	Rough coated	0.07	1220	3.485 (1.6%)	19.91 (7.5%)	44.8 (1.9%)
5	Non-coated	0.38	1505	4.285	14.15	51.2
	Porous coated	0.47	1595	4.557 (6.6%)	12.98 (8.2%)	49.3 (3.7%)

Bejan number ($Be = 1/\left[1 + \left(\dot{S}_{gen,\Delta P}/\dot{S}_{gen,\Delta T}\right)\right]$) exhibits the relative magnitude of irreversibility associated with the temperature difference and pressure drop [60]. In this study, the values of Be number are 0.97, and 0.93 for low and high wall superheats, respectively. From a physical point of view, this suggests that the temperature difference is mostly responsible for exergy destruction at low wall superheat, while the pressure difference also contributes to entropy generation at higher wall superheat.

Exergy destruction due to the pressure difference in flow boiling experiments strongly depends on the distribution of vapor and liquid phases inside the evaporator. Since the bio-coating thicknesses are negligible compared to the tube diameter, the frictional pressure drop in two-phase flows can be considered as the main source for this type of exergy destruction.

The larger exergy losses between evaporator inlet and outlet in the non-coated evaporator are due to i) higher wall temperature required for the onset of nucleate boiling, ii) non-uniform surface temperature due to lower number of active nucleation sites, iii) larger frictional pressure drop due to the presence of larger vapor bubbles [61],[62],[63]. Generated larger bubbles (Figure 4.2) on the non-coated evaporator results in larger bubble slip velocity and higher deformability, which all eventually increase the frictional pressure drop of flow boiling inside the 2-m long evaporator [64].

Exergy destruction due to the temperature difference between the coolant flow and wall temperature occurs during heat transfer. As can be seen in Table 4.1, the evaporator exergy destruction rate decreases with vapor quality for both wall superheat conditions. This means that the temperature difference between the wall and coolant decreases with vapor quality. In other words, the exergy reduction is due to enhancement in boiling heat transfer. Basically, the quality of energy transferred from surface to coolant increases on the coated surfaces because they facilitate the inception of boiling at lower wall temperature (for the low wall superheat case) and uniform surface temperature distribution due to more vapor generation (for higher wall superheat case). Figure 4.4a and 4.4b illustrate the pressure-enthalpy diagrams for the low and high wall superheat experiments, respectively. Under the experimental conditions it can be observed that the rough-coated evaporator enhances the exergy destruction ratio up to 7.5% compared to the non-coated case (as shown in Figure 4.4c). On the other hand, the porous-coated evaporator demonstrates an 8.2% decrease in the exergy destruction ratio compared to the non-coated case (Figure 4.4d). By improving the phase change process, the coated samples generate more vapor inside the evaporator. Therefore, the inlet vapor quality of the condenser is higher for the coated evaporator compared to the non-coated one. As a result, the exergy destruction rate of the condenser is higher for the cycles utilizing modified evaporators.

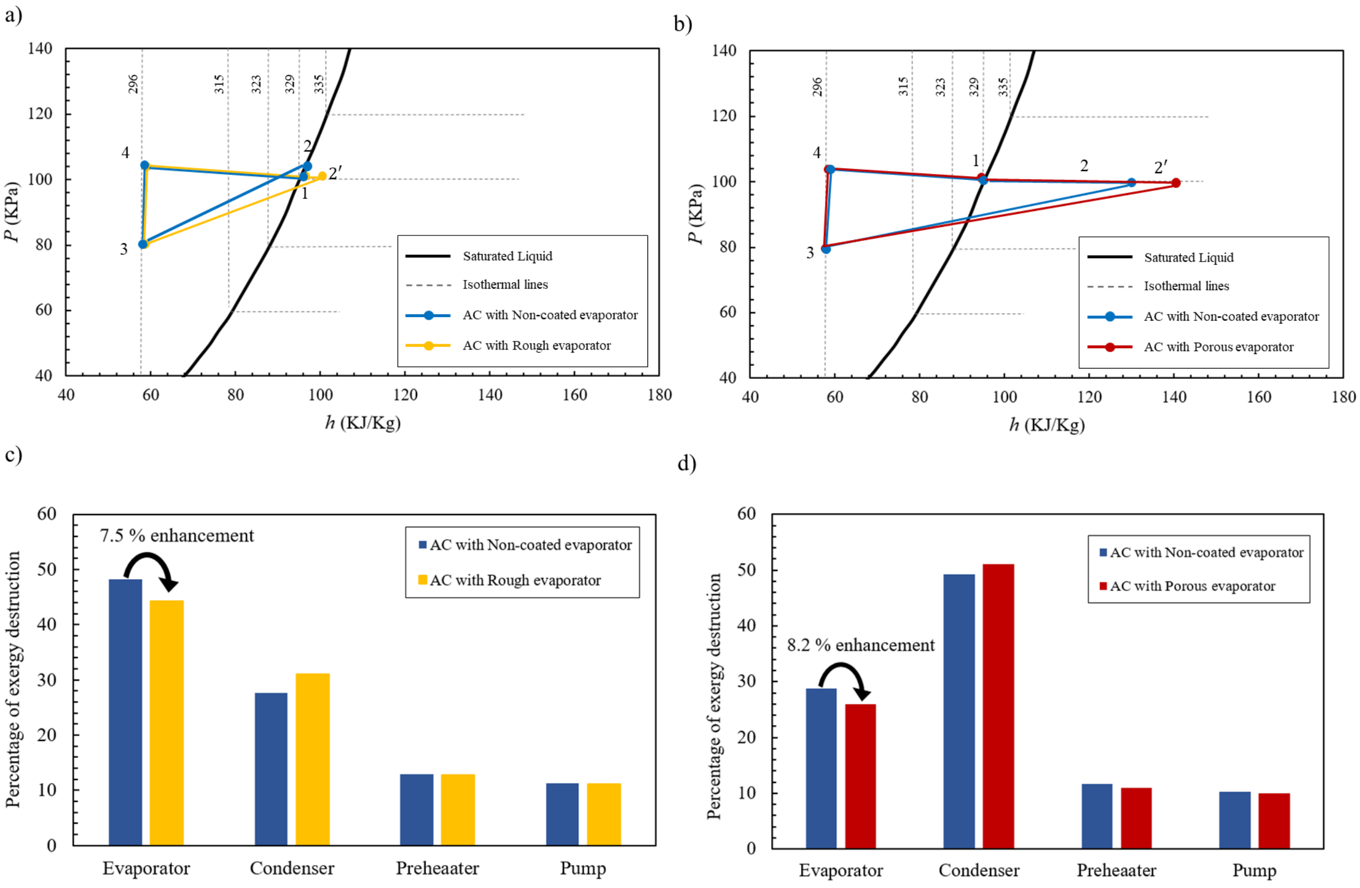

Figure 4.4. a,b) Thermodynamic cycle of pumped two-phase air conditioning system with rough, porous and non-coated evaporators. Here, the rough-coated evaporator was tested and compared to the non-coated evaporator at the wall superheat of 0.5 K, while porous-coated evaporator was tested and compared to the non-coated evaporator at wall superheat of 5 K. c,d) Percentage of exergy destruction in different components of the lab-made air conditioning system with different evaporators.

4.4 Surface roughness effect before applying bio-coating

After grinding the copper and aluminum substrates with different sandpaper grit numbers, they were coated with the bio-material and tested in the pool boiling experimental setup to fundamentally investigate heat transfer performance. The applied roughness on the metallic substrates was measured using Profilometer device and it is tabulated in Table 4.2. It should be mentioned that the bio-coated layer on the metallic surfaces is porous since they have dried in Oven (60°C) after dip-coating. The average thickness of the bio-layer is 1.2 µm (as the same as coatings applied on the previous polished substrates)

Table 4.2. Applied roughness on copper and aluminum surfaces corresponding to different sandpaper grit sizes.

Grit size of the sandpaper	Ra (µm), Aluminum	Ra (µm), Copper
#400	0.73	0.45
#600	0.42	0.18
#800	0.28	0.127
#1000	0.21	0.095
#1200	0.17	0.082
#3000	0.05	0.02

The heat transfer performance of the coated metallic surfaces with artificial roughness is shown in Figure 4.5. The results indicate enhancement in treated surfaces compared to fully polished surface (Grit size #3000). These enhancements are observed both in bubbles nucleation condition (low heat fluxes) and CHF condition (higher heat fluxes). The reason for better enhancement at low heat fluxes are the abundant nucleation sites (below the bio-coated layer) compared to the polished ones and the reason behind better enhancement at higher heat fluxes are the inter-connected micron-size channels through the porous structures of the bio-layer. These tiny bubbles nucleates from beneath of the bio-layer and they move toward the porous structure and this porous layer on top, delay the film boiling condition where the CHF starts.

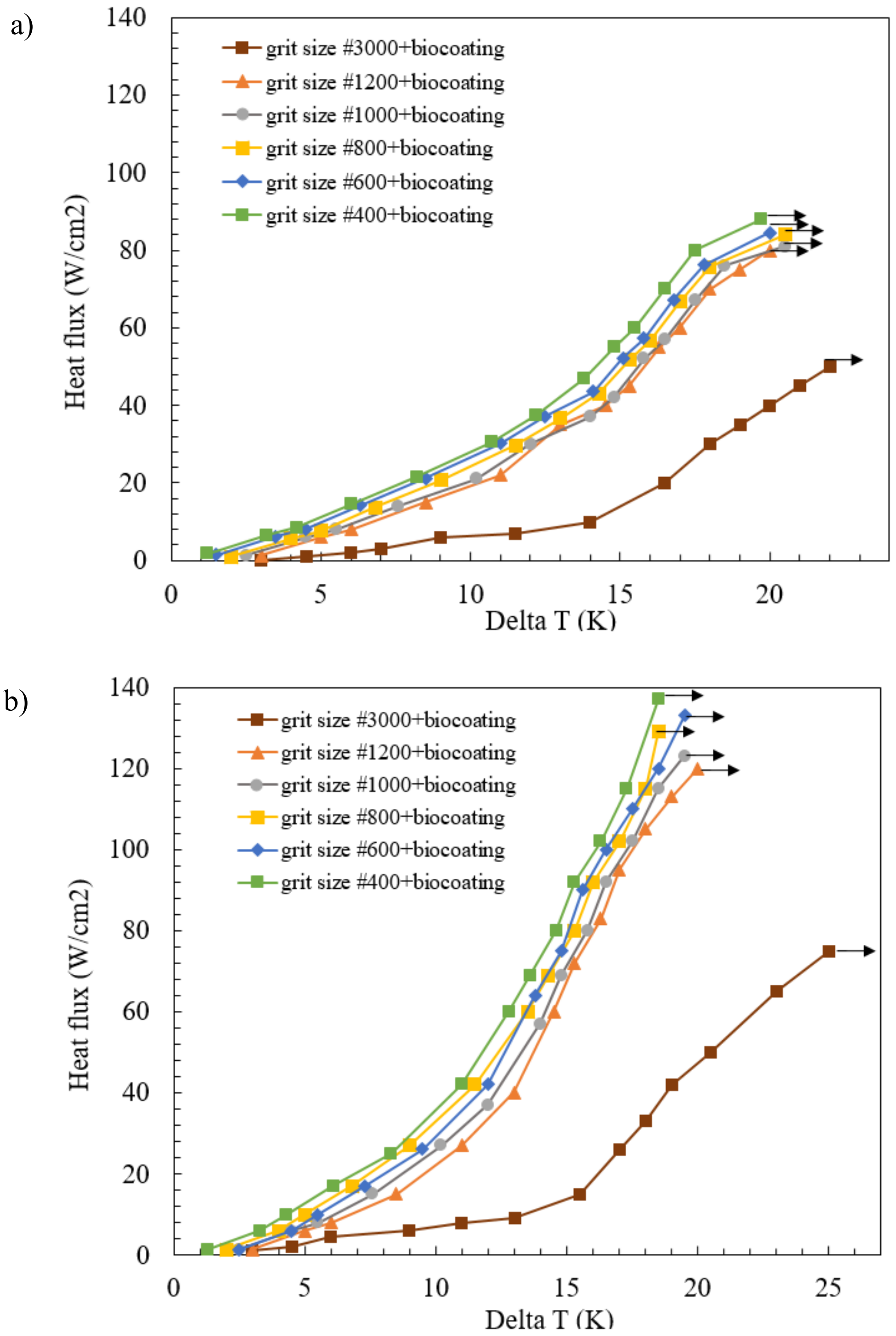

Figure 4.5. Obtained wall superheats as a function of the applied heat flux in pool boiling experimental setup a) On treated aluminum substrates, b) on treated copper substrates.

As the average roughness increases, better enhancement are observed, but the critical point is that the average roughness of the metallic substrate shouldn't exceed the average thickness of the bio-layer. If this condition happens, the bio-material fills the roughness cavities of the surface and the porous bio-layers could not be connected to each other for bubble transfer. As shown in Figure 4.5, superior heat transfer was observed in copper substrates compared to aluminum substrates due to its higher thermal conductivity. Above all of the advantages of using metallic surfaces, they have a drawback that they can be oxidized faster especially when roughness applies on them (compared to polished metals). For porous coating, there is no problem since it is kept in oven just for 1 hour. Whereas, for applying roughness-bio-coating on metallic treated surfaces in room temperature, because it takes longer time (about one day), it is more likely that the metallic surface be oxidized during the evaporation of the biomaterial.

4.5 Cost analysis of the proposed bio-coating

Air conditioning systems - most important energy systems - are one of the largest energy consumers in residential and commercial buildings. In the United States alone 400 terawatt-hours of electricity are consumed annually for air conditioning purposes [65]. Setting higher efficiency standards for cooling devices is one of the approaches, which can dramatically reduce the need for new power plants, cut gas emissions, and reduce the costs. Due to its liquid state and organic properties, the proposed bio-coating offers an unprecedented advantage so that it may be applied by an immersion or rotary coating process, where no external material is used to enhance its durability. These features are major advantages and reduce the overall cost of the proposed technology remarkably. It is expected that for the implementation to 100,000 units, 100 batches/year (250L/batch) of the biomaterial is needed to cover the volume of the industrial evaporators. It is then estimated that every 500 L fermentation batch of the bio-coating medium will be enough to coat approximately 10,000 evaporators.

One of the main disadvantages of the proposed coating is its durability under high temperature conditions or corrosive gases. Heat recovery systems are one of the examples of such applications. The bio-based nature of the coating restricts its applications in the use of bio-degraded materials or under bio-degraded conditions. Our proposed bio-coating to be implemented to air conditioning systems will not only significantly reduce the green-house gas emission but it will also assist in saving billions of dollars.

Here, for the sake of cost analysis, the preparation and coating expenses are provided to support this claim. Raw material expanses for the preparation of the bio-coating and cost of equipment for culture and coating steps are tabulated in Tables 4.3. Each 500L lab-scale batch production will cost around 3500$ and additional €2500$ for the culture and coating apparatus. These calculations yield an approximate manufacturing cost of bio-coating per unit heat exchanger of 0.6 $. Every heat exchanger (2 meter long with the ID of 6mm) requires 56 mL of the biomaterial for a uniform microscale coating. The cost of coating was estimated by the below equation for better estimation of expenses in a surface area coating [66]:

$$\mathbf{Cos\,t\ of\ coating}\left(\frac{\mathbf{USD}}{\mathbf{m^2}}\right) \cong \frac{\mathbf{Cos\,t\ \ of\ raw\ materials(USD) + Preparation\ cost(USD)}}{\mathbf{Area(m^2)}} \tag{4.2}$$

The batch production of this coating method enables it for lowering the expenses especially in the industrial-scale batch culture of the biomaterial. In addition, this coating method offers surface modification before and after manufacturing the heat exchangers and pipes, which shows its advantage compared to other techniques that apply surface modifications before manufacturing of the pipes.

Table 4.3. Cost analysis of the proposed bio-coating.

	Cost for production of 500 L (USD)	Cost for production of 1L (USD)	Cost for coating a heat exchanger (2 meter-long with ID of 6mm) (USD)	Cost of coating (USD/m^2)
Sulfolobus solfataricus (ATCC®)	700	1.4	0.07	1.85
Medium chemicals (Yeast Extract, Casamino Acids, KH_2PO_4, $(NH_4)_2SO_4$, $MgSO_4$, $CaCl_2$, $MnCl_2$, $Na_2B_4O_7$, $ZnSO_4$, $CuCl_2$, Na_2MoO_4, $VOSO_4$, $CoSO_4$)	2000	4	0.2	5.3
Poly-Lysine solution	800	1.6	0.08	2.12
Culturing apparatus	1000	2	0.1	2.65
Coating apparatus	1000	2	0.1	2.65
Total	6000	12	0.6	15.9

5 CHAPTER FOUR: CONCLUSIONS

5.1 Conclusion

In this thesis, a new class of bio-based surface modification technique for thermal-fluid applications is presented and validated using a heat resistant microorganism, Sulfolobus solfataricus. The proposed bio-coating was cultured and optimized to provide organic roughness and porous coating on the desired metallic and non-metallic substrates. Fundamental studies were performed to investigate the enhancement in flow boiling and pool boiling heat transfer. Afterwards, the coating was successfully adapted and tested in miniature air-conditioning systems for performance assessment. Significant enhancements in performances (based on both first and second laws of thermodynamics) were achieved. According to the obtained results, up to 11% and 3.7% enhancements in the coefficient of performance (COP) and overall exergy destruction of the system were achieved, respectively. Unlike most of the available surface modification techniques, which require expensive microfabrication devices (physical modifications) and have damaging impact on the environment (chemical modifications), the proposed technique is economical, scalable, biocompatible and eco-friendly. In addition, the combination of artificial roughness implemented on metallic surfaces before applying the bio-coating were discussed.

5.2 Future research directions

In this thesis, two temperatures were used as evaporation conditions of the bio-material. More parameters could be considered such as the pore size of the porous structure. More characterization could be done on the bio-coating layer by EDX (Energy Dispersive X-Ray Analysis), XRD (X Ray Diffraction) and other material testing devices. Increasing the durability of the proposed bio-coating is of great importance. Thus, different polymeric solutions could be mixed and studied regarding the bio-material to increase the adhesion of the bio-coting on any desired surface as much as possible.

BIBLIOGRAPHY

[1] International energy agency (IEA), (n.d.). https://www.iea.org/news/air-conditioning-use-emerges-as-one-of-the-key-drivers-of-global-electricity-demand-growth (accessed September 2, 2020).

[2] I. Mudawar, Assessment of high-heat-flux thermal management schemes, IEEE Trans. Components Packag. Technol. 24 (2001) 122–141.

[3] J.R. Thome, Boiling in microchannels: a review of experiment and theory, Int. J. Heat Fluid Flow. 25 (2004) 128–139.

[4] S. Xie, M.S. Beni, J. Cai, J. Zhao, Review of critical-heat-flux enhancement methods, Int. J. Heat Mass Transf. 122 (2018) 275–289.

[5] M.T. Gevari, T. Abbasiasl, S. Niazi, M. Ghorbani, A. Koşar, Direct and indirect thermal applications of hydrodynamic and acoustic cavitation: A review, Appl. Therm. Eng. 171 (2020). https://doi.org/10.1016/j.applthermaleng.2020.115065.

[6] M.T. Gevari, S. Niazi, M. Karimzadehkhouei, K. Sendur, M.P. Menguc, M. Ghorbani, A. Koşar, Deagglomeration of nanoparticle clusters in a “cavitation on chip” device, AIP Adv. 10 (2020) 115204.

[7] D. Attinger, C. Frankiewicz, A.R. Betz, T.M. Schutzius, R. Ganguly, A. Das, C.-J. Kim, C.M. Megaridis, Surface engineering for phase change heat transfer: A review, MRS Energy Sustain. 1 (2014).

[8] M. Shojaeian, A. Koşar, Pool boiling and flow boiling on micro-and nanostructured surfaces, Exp. Therm. Fluid Sci. 63 (2015) 45–73.

[9] U. Kumar, S. Suresh, M.R. Thansekhar, D. Babu, Effect of diameter of metal nanowires on pool boiling heat transfer with FC-72, Appl. Surf. Sci. 423 (2017) 509–520.

[10] Z. Yao, Y.-W. Lu, S.G. Kandlikar, Effects of nanowire height on pool boiling performance of water on silicon chips, Int. J. Therm. Sci. 50 (2011) 2084–2090.

[11] D. Li, G.S. Wu, W. Wang, Y.D. Wang, D. Liu, D.C. Zhang, Y.F. Chen, G.P. Peterson, R. Yang, Enhancing flow boiling heat transfer in microchannels for thermal management with monolithically-integrated silicon nanowires, Nano Lett. 12 (2012) 3385–3390.

[12] E. Demir, T. Izci, A.S. Alagoz, T. Karabacak, A. Koşar, Effect of silicon nanorod length on horizontal nanostructured plates in pool boiling heat transfer with water, Int. J. Therm. Sci. 82 (2014) 111–121.

[13] A.K. Sadaghiani, A.R. Motezakker, S. Kasap, I.I. Kaya, A. Koşar, Foamlike 3D graphene coatings for cooling systems involving phase change, ACS Omega. 3 (2018) 2804–2811.

[14] T. Bharathidasan, S. Sathiyanaryanan, Self-replenishing superhydrophobic durable polymeric nanocomposite coatings for heat exchanger channels in thermal management applications, Prog. Org. Coatings. 148 (2020) 105828.

[15] A. Khalili Sadaghiani, A. Reza Motezakker, A. Volkan Özpınar, G. Özaydın İnce, A. Koşar, Pool boiling heat transfer characteristics of inclined pHEMA-coated surfaces, J. Heat Transfer. 139 (2017).

[16] T. Çıkım, E. Armağan, G. Ozaydin Ince, A. Koşar, Flow Boiling Enhancement in Microtubes With Crosslinked pHEMA Coatings and the Effect of Coating Thickness, J. Heat Transfer. 136 (2014). https://doi.org/10.1115/1.4027352.

[17] M.M. Rahman, E. Ölçeroğlu, M. McCarthy, Scalable Nanomanufacturing of Virus-templated Coatings for Enhanced Boiling, Adv. Mater. Interfaces. 1 (2014) 1300107.

[18] A.R. Motezakker, A.K. Sadaghiani, S. Çelik, T. Larsen, L.G. Villanueva, A. Koşar, Optimum ratio of hydrophobic to hydrophilic areas of biphilic surfaces in thermal fluid systems involving boiling, Int. J. Heat Mass Transf. 135 (2019) 164–174.

[19] C.M. Patil, S.G. Kandlikar, Review of the manufacturing techniques for porous surfaces used in enhanced pool boiling, Heat Transf. Eng. 35 (2014) 887–902.

[20] P. Xu, Q. Li, Y. Xuan, Enhanced boiling heat transfer on composite porous surface, Int. J. Heat Mass Transf. 80 (2015) 107–114.

[21] M. Može, M. Senegačnik, P. Gregorčič, M. Hočevar, M. Zupančič, I. Golobič, Laser-Engineered Microcavity Surfaces with a Nanoscale Superhydrophobic Coating for Extreme Boiling Performance, ACS Appl. Mater. Interfaces. 12 (2020) 24419–24431.

[22] H. Bostanci, V. Singh, J.P. Kizito, D.P. Rini, S. Seal, L.C. Chow, Microscale surface modifications for heat transfer enhancement, ACS Appl. Mater. Interfaces. 5 (2013) 9572–9578.

[23] A. Ma, J. Wei, M. Yuan, J. Fang, Enhanced flow boiling heat transfer of FC-72 on micro-pin-finned surfaces, Int. J. Heat Mass Transf. 52 (2009) 2925–2931.

[24] A.K. Sadaghiani, N.S. Saadi, S.S. Parapari, T. Karabacak, M. Keskinoz, A. Koşar, Boiling heat transfer performance enhancement using micro and nano structured surfaces for high heat flux electronics cooling systems, Appl. Therm. Eng. 127 (2017) 484–498.

[25] T. Alam, P.S. Lee, C.R. Yap, Effects of surface roughness on flow boiling in silicon microgap heat sinks, Int. J. Heat Mass Transf. 64 (2013) 28–41.

[26] J.-Y. Jung, H.-Y. Kwak, Effect of surface condition on boiling heat transfer from silicon chip with submicron-scale roughness, Int. J. Heat Mass Transf. 49 (2006) 4543–4551.

[27] Y. Şişman, A.K. Sadaghiani, K.R. Khedir, M. Brozak, T. Karabacak, A. Koşar, Subcooled flow boiling over microstructured plates in rectangular minichannels, Nanoscale Microscale Thermophys. Eng. 20 (2016) 173–190.

[28] K.N. Rainey, G. Li, S.M. You, Flow boiling heat transfer from plain and microporous coated surfaces in subcooled FC-72, J. Heat Transf. 123 (2001) 918–925.

[29] M.S. Sarwar, Y.H. Jeong, S.H. Chang, Subcooled flow boiling CHF enhancement with porous surface coatings, Int. J. Heat Mass Transf. 50 (2007) 3649–3657.

[30] C.Y. Zhao, W. Lu, S.A. Tassou, Flow boiling heat transfer in horizontal metal-foam tubes, J. Heat Transfer. 131 (2009).

[31] I. Pranoto, K.C. Leong, An experimental study of flow boiling heat transfer from porous foam structures in a channel, Appl. Therm. Eng. 70 (2014) 100–114.

[32] Paints and Coatings Market Size, Trends, Share, Report 2027., (n.d.). https://www.fortunebusinessinsights.com (accessed August 28, 2020).

[33] S. Niazi, A.K. Sadaghiani, G. Gharib, V.O. Kaya, S. Çelik, Ö. Kutlu, A. Koşar, Bio-coated surfaces with micro-roughness and micro-porosity: Next generation coatings for enhanced energy efficiency, Energy. 222 (2021). https://doi.org/10.1016/j.energy.2021.119959.

[34] M. V Sardeshpande, V. V Ranade, Two-phase flow boiling in small channels: A brief review, Sadhana. 38 (2013) 1083–1126.

[35] F.C. McQuiston, J.D. Parker, J.D. Spitler, Heating, ventilating, and air conditioning: analysis and design, John Wiley & Sons, 2004.

[36] I. Dincer, M. Kanoglu, Refrigeration systems and applications, Wiley Online Library, 2010.

[37] Technical data sheets and data tables for saturated FC-72. 3M Corporation (3M^{TM} Fluorinert^{TM} Electronic Liquid), (n.d.).

[38] H.W. Coleman, W.G. Steele, Experimentation, validation, and uncertainty analysis for engineers, John Wiley & Sons, 2018.

[39] M. Ciaramella, F.M. Pisani, M. Rossi, Molecular biology of extremophiles: recent progress on the hyperthermophilic archaeon Sulfolobus, Antonie Van Leeuwenhoek. 81 (2002) 85–

97.

[40] B. Chaban, S.Y.M. Ng, K.F. Jarrell, Archaeal habitats—from the extreme to the ordinary, Can. J. Microbiol. 52 (2006) 73–116.

[41] C. Schleper, G. Puehler, I. Holz, A. Gambacorta, D. Janekovic, U.T.E. Santarius, H.-P. Klenk, W. Zillig, Picrophilus gen. nov., fam. nov.: a novel aerobic, heterotrophic, thermoacidophilic genus and family comprising archaea capable of growth around pH 0., J. Bacteriol. 177 (1995) 7050–7059.

[42] K. Kashefi, D.R. Lovley, Extending the Upper Temperature Limit for Life, Science (80-.). 301 (2003) 934 LP – 934. https://doi.org/10.1126/science.1086823.

[43] D.W. Grogan, Phenotypic characterization of the archaebacterial genus Sulfolobus: comparison of five wild-type strains., J. Bacteriol. 171 (1989) 6710 LP – 6719. https://doi.org/10.1128/jb.171.12.6710-6719.1989.

[44] S. Ohki, K.B.T.-M. in E. Arnold, Determination of Liposome Surface Dielectric Constant and Hydrophobicity, in: Liposomes, Part A, Academic Press, 2003: pp. 253–272. https://doi.org/https://doi.org/10.1016/S0076-6879(03)67016-3.

[45] X. Wang, G. Cai, L. Fu, Y. Wu, X. Wang, B. Ren, H. Ma, A proton shelter inspired by the sugar coating of acidophilic archaea, Sci. Rep. 2 (2012) 1–5.

[46] N. Allocati, M. Masulli, C. Di Ilio, V. De Laurenzi, Die for the community: an overview of programmed cell death in bacteria, Cell Death Dis. 6 (2015) e1609–e1609.

[47] G. Simon, J. Walther, N. Zabeti, Y. Combet-Blanc, R. Auria, J. Van Der Oost, L. Casalot, Effect of O2 concentrations on Sulfolobus solfataricus P2, FEMS Microbiol. Lett. 299 (2009) 255–260.

[48] T. Ulas, S.A. Riemer, M. Zaparty, B. Siebers, D. Schomburg, Genome-scale reconstruction and analysis of the metabolic network in the hyperthermophilic archaeon Sulfolobus solfataricus, PLoS One. 7 (2012) e43401.

[49] P.H. Clarke, Hydrogen sulphide production by bacteria, Microbiology. 8 (1953) 397–407.

[50] B.B. Jørgensen, Mineralization of organic matter in the sea bed—the role of sulphate reduction, Nature. 296 (1982) 643–645.

[51] G.W. Luther, A.J. Findlay, D.J. MacDonald, S.M. Owings, T.E. Hanson, R.A. Beinart, P.R. Girguis, Thermodynamics and kinetics of sulfide oxidation by oxygen: a look at inorganically controlled reactions and biologically mediated processes in the environment,

Front. Microbiol. 2 (2011) 62.

[52] D.E. Canfield, B. Thamdrup, The production of 34S-depleted sulfide during bacterial disproportionation of elemental sulfur, Science (80-.). 266 (1994) 1973–1975.

[53] X. Chen, T.J. Andersen, Y. Morono, F. Inagaki, B.B. Jørgensen, M.A. Lever, Bioturbation as a key driver behind the dominance of Bacteria over Archaea in near-surface sediment, Sci. Rep. 7 (2017) 1–14.

[54] X. Chen, X. Wang, P.G. Chen, Q. Liu, Determination of diffusion coefficient in droplet evaporation experiment using response surface method, Microgravity Sci. Technol. 30 (2018) 675–682.

[55] Solubility of Gases in Water, (n.d.). https://www.engineeringtoolbox.com (accessed September 2, 2020).

[56] A.R. Motezakker, A.K. Sadaghiani, Y. Akkoc, S.S. Parapari, D. Gözüaçık, A. Koşar, Surface modifications for phase change cooling applications via crenarchaeon Sulfolobus solfataricus P2 bio-coatings, Sci. Rep. 7 (2017) 1–9.

[57] A.K. Sadaghiani, R. Altay, H. Noh, H.J. Kwak, K. Şendur, B. Mısırlıoğlu, H.S. Park, A. Koşar, Effects of bubble coalescence on pool boiling heat transfer and critical heat flux–A parametric study based on artificial cavity geometry and surface wettability, Int. J. Heat Mass Transf. 147 (2020) 118952.

[58] S. Sanaye, M.M. Ghafurian, F.T. Dastjerd, Applying Relative Net Present or Relative Net Future Worth Benefit and exergy efficiency for optimum selection of a natural gas engine based CCHP system for a hotel building, J. Nat. Gas Sci. Eng. 34 (2016) 305–317.

[59] M.M. Ghafurian, H. Niazmand, New approach for estimating the cooling capacity of the absorption and compression chillers in a trigeneration system, Int. J. Refrig. 86 (2018) 89–106.

[60] M.M. Awad, A review of entropy generation in microchannels, Adv. Mech. Eng. 7 (2015) 1687814015590297.

[61] C.A. Chávez, H.L.S.L. Leão, G. Ribatski, Evaluation of thermal-hydraulic performance of hydrocarbon refrigerants during flow boiling in a microchannels array heat sink, Appl. Therm. Eng. 111 (2017) 703–717.

[62] M.-H. Yang, R.-H. Yeh, Performance and exergy destruction analyses of optimal subcooling for vapor-compression refrigeration systems, Int. J. Heat Mass Transf. 87 (2015)

1–10.

[63] M. Karimzadehkhouei, M. Shojaeian, A.K. Sadaghiani, K. Şendur, M.P. Mengüç, A. Koşar, Entropy generation analysis of laminar flows of water-based nanofluids in horizontal minitubes under constant heat flux conditions, Entropy. 20 (2018) 242.

[64] Y. Murai, Frictional drag reduction by bubble injection, Exp. Fluids. 55 (2014) 1773.

[65] L.T. Biardeau, L.W. Davis, P. Gertler, C. Wolfram, Heat exposure and global air conditioning, Nat. Sustain. 3 (2020) 25–28.

[66] M.M. Ghafurian, H. Niazmand, E.K. Goharshadi, B.B. Zahmatkesh, A.E. Moallemi, R. Mehrkhah, O. Mahian, Enhanced solar desalination by delignified wood coated with bimetallic Fe/Pd nanoparticles, Desalination. 493 (2020) 114657.